UWS Academic Portal

High-spin structure in the transitional nucleus 131Xe

Kaya, L.; Vogt, A.; Reiter, P.; Siciliano, M.; Birkenbach, B.; Blazhev, A.; Coraggio, L.; Teruya, E.; Yoshinaga, N.; Higashiyama, K.; Arnswald, K.; Bazzacco, D.; Bracco, A.; Bruyneel, B.; Corradi, L.; Crespi, F.C.L.; de Angelis, G.; Eberth, J.; Farnea, E.; Fioretto, E.; Fransen, C.; Fu, B.; Gadea, A.; Gargano, A.; Giaz, A.; Görgen, A.; Gottardo, A.; Hadyska-Klk, K.; Hess, H.; Hetzenegger, R.; Hirsch, R.; Itaco, N.; John, P.R.; Jolie, J.; Jungclaus, A.; Korten, W.; Leoni, S.; Lewandowski, L.; Lunardi, S.; Menegazzo, R.; Mengoni, D.; Michelagnoli, C.; Mijatovi, T. ; Montagnoli, G.; Montanari, D.; Müller-Gatermann, C.; Napoli, D.; Podolyák, Zs.; Pollarolo, G.; Pullia, A.; Queiser, M.; Recchia, F.; Rosiak, D.; Saed-Samii, N.; ahin, E.; Scarlassara, F.; Schneiders, D.; Seidlitz, M.; Siebeck, B.; Smith, J.F. ; Söderström, P.-A.; Stefanini, A.M.; Steinbach, T.; Stezowski, O.; Szilner, S.; Szpak, B.; Ur, C.; Valiente-Dobón, J.J.; Wolf, K.; Zell, K.O.

Published in:
Physical Review C

DOI:
10.1103/PhysRevC.98.014309

Published: 06/07/2018

Document Version
Peer reviewed version

Citation for published version (APA):
Kaya, L., Vogt, A., Reiter, P., Siciliano, M., Birkenbach, B., Blazhev, A., ... Zell, K. O. (2018). High-spin structure in the transitional nucleus 131Xe: Competitive neutron and proton alignment in the vicinity of the N = 82 shell closure. Physical Review C, 98(1), [014309]. https://doi.org/10.1103/PhysRevC.98.014309

High-spin structure in the transitional nucleus ^{131}Xe: Competitive neutron and proton alignment in the vicinity of the N = 82 shell closure

L. Kaya,[1,a] A. Vogt,[1] P. Reiter,[1] M. Siciliano,[2,3] B. Birkenbach,[1] A. Blazhev,[1] L. Coraggio,[4] E. Teruya,[5] N. Yoshinaga,[5] K. Higashiyama,[6] K. Arnswald,[1] D. Bazzacco,[7] A. Bracco,[8] B. Bruyneel,[9] L. Corradi,[3] F. C. L. Crespi,[8] G. de Angelis,[3] J. Eberth,[1] E. Farnea,[7,b] E. Fioretto,[3] C. Fransen,[1] B. Fu,[1] A. Gadea,[10] A. Gargano,[4] A. Giaz,[8] A. Görgen,[11,12,13] A. Gottardo,[3] K. Hadyńska-Klęk,[3] H. Hess,[1] R. Hetzenegger,[1] R. Hirsch,[1] N. Itaco,[4,14] P. R. John,[15] J. Jolie,[1] A. Jungclaus,[16] W. Korten,[17] S. Leoni,[8] L. Lewandowski,[1] S. Lunardi,[2,7] R. Menegazzo,[7] D. Mengoni,[18,2,7] C. Michelagnoli,[19] T. Mijatović,[20] G. Montagnoli,[2,7] D. Montanari,[2,7] C. Müller-Gatermann,[1] D. Napoli,[3] Zs. Podolyák,[21] G. Pollarolo,[22] A. Pullia,[8] M. Queiser,[1] F. Recchia,[2,7] D. Rosiak,[1] N. Saed-Samii,[1] E. Şahin,[23] F. Scarlassara,[2,7] D. Schneiders,[1] M. Seidlitz,[1] B. Siebeck,[1] J. F. Smith,[24] P.-A. Söderström,[25] A. M. Stefanini,[3] T. Steinbach,[1] O. Stezowski,[26] S. Szilner,[20] B. Szpak,[27] C. Ur,[7] J. J. Valiente-Dobón,[3] K. Wolf,[1] and K. O. Zell[1]

[1] *Institut für Kernphysik, Universität zu Köln, D-50937 Köln, Germany*
[2] *Dipartimento di Fisica e Astronomia, Università di Padova, I-35131 Padova, Italy*
[3] *Istituto Nazionale di Fisica Nucleare, Laboratori Nazionali di Legnaro, I-35020 Legnaro, Italy*
[4] *Istituto Nazionale di Fisica Nucleare, Sezione di Napoli, I-80126 Napoli, Italy*
[5] *Department of Physics, Saitama University, Saitama City 338-8570, Japan*
[6] *Department of Physics, Chiba Institute of Technology, Narashino, Chiba 275-0023, Japan*
[7] *Istituto Nazionale di Fisica Nucleare, Sezione di Padova, I-35131 Padova, Italy*
[8] *Dipartimento di Fisica, Università di Milano and INFN Sezione di Milano, I-20133 Milano, Italy*
[9] *CEA Saclay, Service de Physique Nucleaire, F-91191 Gif-sur-Yvette, France*
[10] *Instituto de Física Corpuscular, CSIC-Universidad de Valencia, E-46071 Valencia, Spain*
[11] *Department of Physics, University of Oslo, P. O. Box 1048 Blindern, N-0316 Oslo, Norway*
[12] *Institut de Recherche sur les lois Fondamentales de l'Univers – IRFU, CEA/DSM, Centre CEA de Saclay, F-91191 Gif-sur-Yvette Cedex, France*
[13] *Lawrence Berkeley National Laboratory, Berkeley, California 94720, USA*
[14] *Dipartimento di Matematica e Fisica, Universitá degli Studi della Campania "Luigi Vanvitelli", viale A. Lincoln 5, I-8110 Caserta, Italy*
[15] *Institut für Kernphysik, Technische Universität Darmstadt, D-64289 Darmstadt, Germany*
[16] *Instituto de Estructura de la Materia, CSIC, Madrid, E-28006 Madrid, Spain*
[17] *IRFU, CEA, Universitè Paris-Saclay, F-91191 Gif-sur-Yvette, France*
[18] *Nuclear Physics Research Group, University of the West of Scotland, High Street, Paisley PA1 2BE, Scotland, United Kingdom*
[19] *Institut Laue-Langevin (ILL), 38042 Grenoble Cedex 9, France.*
[20] *Ruđer Bošković Institute, HR-10 002 Zagreb, Croatia*
[21] *Department of Physics, University of Surrey, Guildford, Surrey GU2 7XH, United Kingdom*
[22] *Dipartimento di Fisica Teorica dell'Università di Torino and INFN, I-10125 Torino, Italy*
[23] *Department of Physics, University of Oslo, P. O. Box 1048 Blindern, N-0316 Oslo, Norway.*
[24] *SUPA, School of Engineering and Computing, University of the West of Scotland, Paisley PA1 2BE, United Kingdom*
[25] *Extreme Light Infrastructure-Nuclear Physics (ELI-NP), 077125 Bucharest-Magurele, Romania*
[26] *Université de Lyon, Université Lyon-1, CNRS/IN2P3, UMR5822, IPNL, F-69622 Villeurbanne Cedex, France*
[27] *Henryk Niewodniczański Institute of Nuclear Physics PAN, PL-31342 Kraków, Poland*

(Dated: June 20, 2018)

The transitional nucleus ^{131}Xe is investigated after multinucleon transfer (MNT) in the ^{136}Xe+^{208}Pb and ^{136}Xe+^{238}U reactions employing the high-resolution Advanced GAmma Tracking Array (AGATA) coupled to the magnetic spectrometer PRISMA at the Laboratori Nazionali di Legnaro, Italy and as an elusive reaction product in the fusion-evaporation reaction ^{124}Sn(^{11}B,$p3n$)^{131}Xe employing the HORUS γ-ray array coupled to a double-sided silicon strip detector (DSSSD) at the University of Cologne, Germany. The level scheme of ^{131}Xe is extended to 5 MeV. A pronounced backbending is observed at $\hbar\omega \approx 0.4$ MeV along the negative-parity one-quasiparticle $\nu h_{11/2}(\alpha = -1/2)$ band. The results are compared to the high-spin systematics of the $Z = 54$ isotopes and the $N = 77$ isotones. Large-scale shell-model calculations (LSSM) employing the PQM130, SN100PN, GCN50:82, SN100-KTH and a realistic effective interaction reproduce the experimental findings and provide guidance to elucidate the structure of the high-spin states. Further calculations in $^{129-132}$Xe provide insight into the changing nuclear structure along the Xe chain towards the $N = 82$ shell closure. Proton occupancy in the $\pi\, 0h_{11/2}$ orbital is found to be decisive for the description of the observed backbending phenomenon.

PACS numbers: 23.20.Lv, 27.60.+j, 29.40.Gx,

I. INTRODUCTION

The nuclei in the $50 \leq Z, N \leq 82$ region of the Segrè chart, spanning the nuclei north-west of doubly-magic ^{132}Sn, are intriguing systems for the simultaneous investigation of the shell structure as well as for collective degrees of freedom. Couplings of configurations involving the unique-parity high-j orbital $0h_{11/2}$ with configurations in the $2s_{1/2}$, $1d_{3/2}$, $1d_{5/2}$, and $0g_{7/2}$ orbitals give rise to a plethora of high-spin states. The different deformation-driving properties of aligned $h_{11/2}$ proton ($\gamma \approx 0°$ in the Lund convention) or neutron ($\gamma \approx -60°$) configurations cause both collective and non-collective structures [1–5]. Transitional Xe nuclei in the $A \approx 130$ mass region, well described by assuming anharmonic vibrations [6], are known for their softness with respect to γ deformation and form therefore an important link in the smooth evolution from spherical to deformed shapes [7–9]. High-j couplings in the high-spin regime form a variety of rotational bands. Their signature splitting ($\alpha = \pm 1/2$) [10] is based on the unique-parity $h_{11/2}$ neutron-hole orbital. Many of the $A \approx 130$ nuclei show irregular yrast sequences in the high-spin regime, accompanied by a sudden increase of moment of inertia along the ground-state band. This phenomenon called backbending [11] is explained as a band crossing of the ground-state band with an aligned two-quasiparticle band, i.e. the quasiparticle level crossing between an unoccupied high-j intruder orbital and the most high-lying occupied orbital.

In the majority of cases the theoretical investigations of such systems were carried out by means of the Interacting Boson Model (IBM) [9, 12, 13], mean-field methods [2, 14] or the cranked shell model (CSM) [15, 16]. However, Xe isotopes have come within reach of advanced untruncated shell-model calculations, providing stringent tests of the predictive power and suitability of various nuclear potentials and models based on modern effective interactions in this region. Is is noteworthy that only a few studies were performed from the shell-model point of view for the description of the backbending [17–19].

The nucleus ^{131}Xe is located in the proton midshell between the $Z = 50$ shell and the $Z = 64$ sub-shell closures and is five neutrons away from the $N = 82$ shell closure. Previous experiments on ^{131}Xe focused primarily on low-spin excitations observed after β decay [20–23], (γ, γ') [24–26] reactions or Coulomb excitation [27]. Like several odd-mass $50 \leq Z, N \leq 82$ nuclei, ^{131}Xe exhibits a long-lived $J^\pi = 11/2^-_1$ isomer. It has a half-life of 11.84(4) d and an excitation energy of 163.930(8) keV. The isomer has a predominant $\nu h^{-1}_{11/2}$ character and decays via an $M4$ γ ray to the $J^\pi = 3/2^+_1$ ground state [28]. By the end of the 1970s, both Palmer *et al.* [27] and Irving *et al.* [29] studied low-lying positive-parity states in ^{131}Xe utilizing Coulomb excitation and $(\alpha, xn\gamma)$ reactions, respectively. Later, in 1983, Lönnroth *et al.* [30] identified a large number of new low-lying states with one- and three-quasiparticle configurations. Due to a lack of stable beam and target combinations, studies of intermediate and high-spin states were restricted by $(\alpha, xn\gamma)$ reactions [29–31] with small Ge(Li) detector arrays at this time. The most detailed spectroscopy study of the high-spin regime was performed by Kerek *et al.* [31] in 1971 utilizing the ^{130}Te(α,3n) reaction at beam energies of 30 to 40 MeV. Three γ rays with energies of 642.4, 810.6 and 901.5 keV on top of the $J^\pi = 11/2^-_1$ state were found to form a $(21/2^-_1) \xrightarrow{901.5} 19/2^-_1 \xrightarrow{810.6} 15/2^-_1 \xrightarrow{642.4} 11/2^-_1$ negative-parity band. Furthermore, three γ rays with energies of 188.7, 389.0 and 991.6 keV were placed on top of the $J^\pi = 19/2^-_1$ state. The 188.7-keV transition was observed as the $19/2^+_1 \rightarrow 19/2^-_1$ decay of the positive-parity band. The $J^\pi = 19/2^+_1$ state at 1805.7 keV was identified as an isomer with a half-life of 14(3) ns and a three-quasiparticle $\nu(h^{-2}_{11/2} s^{-1}_{1/2})$ configuration. The $J^\pi = 23/2^+_1$ state at 2194.7 keV is explained as a $\nu(h^{-2}_{11/2} d^{-1}_{3/2})$ configuration.

Backbending and upbending phenomena in the yrast bands of even-even Xe isotopes were systematically observed in $^{112-130}$Xe [33–35]. Figure 1 shows the evolution of the total aligned angular momentum for a given transition $I_x = (I^i_x + I^f_x)/2$ with the total angular momenta of the initial and final states $I^{i,f}_x = \sqrt{I^{i,f}(I^{i,f}+1) - K^2}$ versus the rotational frequency $\hbar\omega = (E_i - E_f)/(I^i_x - I^f_x)$ [36] for Xe isotopes with masses ranging from $A = 117$ to $A = 132$ along the yrast bands [32]. The experimental total aligned angular momentum shows a smooth evolution as a function of rotational frequency $\hbar\omega$ for the lighter midshell isotopes. Towards the shell closure, backbending emerges between the $J^\pi = 10^+_1$ and $J^\pi = 12^+_1$ states in ^{122,124,126}Xe and between the $J^\pi = 8^+_1$ and $J^\pi = 10^+_1$ states in ^{128,130}Xe. This behavior is explained by the crossing of a quasi ground band and another quasiband with a neutron-aligned $\nu h^{-2}_{11/2}$ configuration [35]. A distinct alignment is observed in the lower-mass neighbor of ^{131}Xe, ^{130}Xe, where the energy difference between the $J^\pi = 10^+_1$ and $J^\pi = 8^+_1$ states is only 276 keV. In the higher-mass neighbor of ^{131}Xe, ^{132}Xe, the $J^\pi = 6^+_1$ state is still tentative and the $J^\pi = 8^+_1$ state is unknown. Compared to the even-mass neighbors of ^{132}Xe, the decay of the $J^\pi = 10^+_1$ state is remarkably hindered ($T_{1/2} = 8.39(11)$ ms [37]). A fully-aligned $\nu h^{-2}_{11/2}$ two neutron-hole configuration was assigned to the state [38]. The $J^\pi = 10^+_1$ state decays predominantly via an $E3$ γ ray to the $J^\pi = (7^-_1)$ state, competitive $E2$ decays were not observed yet. Consequently, it is likely that the $J^\pi = 8^+_1$ state is located very close in energy to the $J^\pi = 10^+_1$ isomer, resulting in a pronounced backbending. This assumption is supported by shell-model calculations [39]. To shade light on the nuclear structure of ^{132}Xe around the $J^\pi = 10^+_1$ state, the high-spin struc-

[a] Corresponding author: levent.kaya@ikp.uni-koeln.de
[b] Deceased.

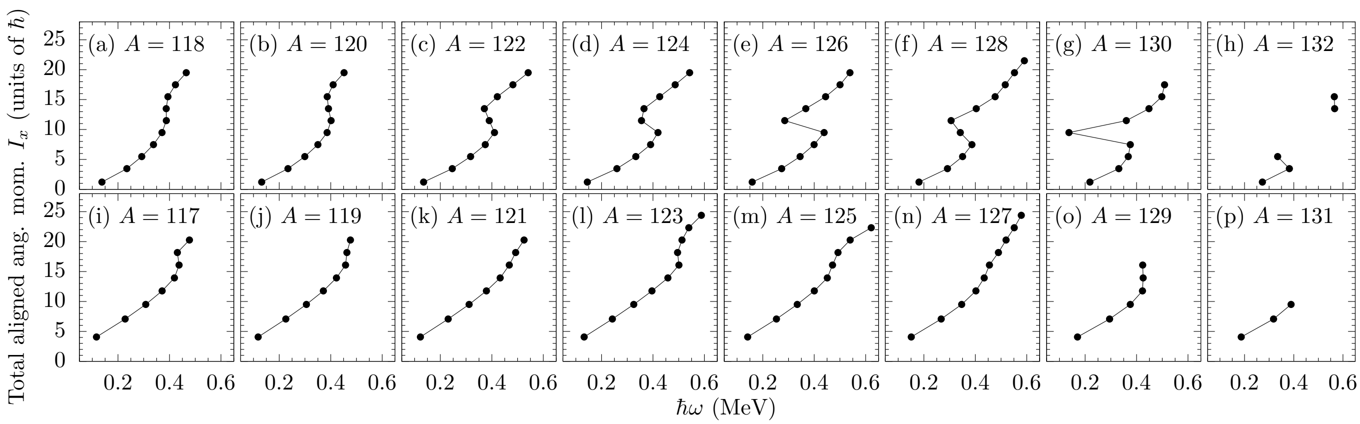

Figure 1. Total aligned angular momentum against the rotational frequency $\hbar\omega$ for the yrast bands in the Xe isotopes with masses ranging from $A = 117$ to $A = 132$. For definitions see text. Going towards the $N = 82$ shell closure, backbending occurs between the $J^\pi = 10^+_1$ and 12^+_1 states in ^{126}Xe and between the $J^\pi = 8^+_1$ and $J^\pi = 10^+_1$ states in ^{128,130}Xe. In ^{132}Xe the position of the $J^\pi = 8^+_1$ state is not known to date. Data extracted from Ref. [32].

.

tures of the odd-mass neighboring nuclei can be used to investigate the inert core ^{132}Xe by means of a semiclassical description within the particle-plus-rotor picture. In ^{133}Xe the single-particle character dominates over the collective character [39].

For the lower odd-mass neighbors of ^{131}Xe, ^{125}Xe and ^{127}Xe, both low-spin structures from ^{3}He- and α-induced reactions [40, 41] and elaborate high-spin information from heavy-ion reactions are available. High-spin states of ^{125}Xe were studied at the OSIRIS Compton-suppressed γ-ray spectrometer via the ^{116}Cd(^{13}C,4n) reaction by Granderath *et al.* [42] and via the ^{48}Ca(^{82}Se,5n) reaction by Wiedenhöver *et al.* [43] up to 8.7 MeV. Later, the level scheme and high-spin band structures were significantly extended by Moon *et al.* [15] and Al-Khatib *et al.* [44], respectively. The favored $(\pi = -1, \alpha = -1/2)$ negative-parity yrast band built on the $J^\pi = 11/2^-_1$ state is known up to $J^\pi = (47/2^-)$. An alignment at a frequency of $\hbar\omega \approx 0.48$ MeV was observed. Granderath *et al.* [42] proposed a triaxial deformation in the negative-parity band according to calculations in the framework of the triaxial rotor-plus-particle (TRP) model. The crossing in the $(\pi = -1, \alpha = -1/2)$ band was assigned to an alignment of a second pair of $h_{11/2}$ neutrons according to theoretical Routhians from CSM calculations. The alignment of the first pair of $h_{11/2}$ neutrons was assumed to be blocked. The findings were reproduced by Moon *et al.* [15] who assigned the negative-parity yrast band a $\nu h_{11/2}$ [523] 7/2 Nilsson configuration from total Routhian surface (TRS) and CSM calculations.

In ^{127}Xe, high-spin states were throroughly studied after ^{48}Ca(^{82}Se,3n) reactions at 275 MeV [43]. The negative-parity ground-state band was extended up to 9.5 MeV and a spin of $J^\pi = (51/2^-)$. A band crossing was observed at slightly lower frequencies compared to ^{125}Xe. This observation corroborated a $\nu h^{-3}_{11/2}$ neutron alignment similar to ^{125}Xe [45], however, no theoretical description is available in the literature to date.

Going towards the $N = 82$ shell closure, ^{129}Xe is the last nucleus which can still be sufficiently populated by means of heavy-ion reactions with stable beams heavier than $A = 4$. In 2016, Huang *et al.* [16] extended the level scheme of the negative-parity ground-state band $(\alpha = -1/2)$ up to the $J^\pi = 35/2^-_1$ state at 5194 keV utilizing a ^{9}Be-induced fusion-evaporation reaction on a ^{124}Sn target at a beam energy of 36 MeV. The Nilsson configuration for the band was determined to be $\nu h_{11/2}$ [505] 11/2. An alignment in the negative-parity ground-state band was found at a crossing frequency of approx. $\hbar\omega \approx 0.45$ MeV. Cranked shell-model calculations predicted an alignment of two $h_{11/2}$ protons at $\hbar\omega \approx 0.5$ MeV. However, the alignment of two $h_{11/2}$ neutrons was predicted at $\hbar\omega \approx 0.27$ MeV. Since the proton crossing frequency matched the experimental observation, the backbending was explained as an alignment of two $h_{11/2}$ protons. Furthermore, particle-plus-rotor model calculations suggested a triaxial deformation with $\gamma \approx -30°$ in the negative-parity ground-state band.

This work focuses on the hitherto unknown high-spin structures above the 2518-keV state in the negative-parity band in ^{131}Xe. Excited states in ^{131}Xe were populated in three different experiments. Multinucleon-transfer reactions have proved to be an efficient way for the population of intermediate to high-spin states. The combination of the high-resolution position-sensitive Advanced GAmma Tracking Array (AGATA) [46] and the PRISMA magnetic mass spectrometer [47–49] at the Laboratori Nazionali di Legnaro (LNL, Italy) was employed to study transitions in ^{131}Xe after ^{136}Xe + ^{208}Pb and ^{136}Xe + ^{238}U multinucleon transfer. Furthermore, ^{131}Xe was populated in a ^{124}Sn(^{11}B, $p3n$)^{131}Xe fusion-evaporation reaction employing the High-efficiency Observatory for γ-Ray Unique Spectroscopy (HORUS) [50] at the Institute of Nuclear Physics, University of Cologne. The γ-ray array was coupled to a double-sided silicon strip detector (DSSSD) [51] for the detection of evaporated protons.

This paper is organized as follows: the experimental setup and data analysis of the three experiments are described in Sec. II, followed by the experimental results in Sec. III. A comparison with results from modern shell-model calculations is presented in Sec. IV before the paper closes with a summary and conclusions in Sec. V.

II. EXPERIMENTAL PROCEDURE AND DATA ANALYSIS

A. ^{136}Xe + ^{208}Pb and ^{136}Xe + ^{238}U multinucleon transfer

Excited states in ^{131}Xe were populated in (i) a ^{136}Xe+ ^{208}Pb, and (ii), in a ^{136}Xe + ^{238}U multinucleon-transfer experiment in the five-neutron stripping channel at the Laboratori Nazionali di Legnaro (LNL), Italy. In the first experiment a 6.84 MeV/nucleon ^{136}Xe beam, delivered by the PIAVE+ALPI accelerator complex, impinged onto a 1-mg/cm^2 ^{208}Pb target. The Advanced GAmma Tracking Array (AGATA) [46] was employed in a first demonstrator configuration [52] with nine large-volume electronically segmented high-purity Ge (HPGe) detectors in three triple cryostats [53] to measure γ rays from excited states. The array was placed at a distance of 18.8 cm from the target position. Details on the setup and data analysis are given in Refs. [54, 55]. In the second experiment, the PIAVE+ALPI accelerator provided a ^{136}Xe beam with an energy of 7.35 MeV/nucleon and a beam current of 2 pnA to subsequently bombard two different ^{238}U targets with thicknesses of 1 and 2 mg/cm^2. A 0.8-mg/cm^2 Nb backing faced the beam. AGATA was employed in its full demonstrator configuration with 15 HPGe detectors in five triple cryostats placed in the nominal position, 23.5 cm away from the target. Information on the data analysis of this experiment is comprised in Ref. [56]. In both experiments the light projectile-like reaction fragments of interest were identified by the magnetic spectrometer PRISMA [47–49] placed at the reaction's grazing angle of $\theta_{\rm lab} = 42°$ in the ^{136}Xe + ^{208}Pb experiment and $\theta_{\rm lab} = 50°$ in the ^{136}Xe + ^{238}U experiment, respectively. Pulse-shape analysis of the digitized detector signals was applied to determine the individual interaction points within the HPGe shell [57], allowing the Orsay forward-tracking algorithm [58] to reconstruct the individual γ-ray energies, determine the first interaction point of the γ ray in the germanium and, thus, the emission angle. Together with the kinematic information from PRISMA, a precise Doppler correction was performed on a event-by-event basis.

B. ^{11}B + ^{124}Sn fusion evaporation

Excited states in ^{131}Xe were populated via the fusion-evaporation reaction ^{124}Sn(^{11}B, $p3n$)^{131}Xe. A 54-MeV ^{11}B beam, delivered by the FN Tandem accelerator located at the Institute for Nuclear Physics, University of Cologne, impinged onto a 3-mg/cm^2 95.3%-enriched ^{124}Sn target which was evaporated on a 2.7-mg/cm^2 $^{\rm nat.}$Ta backing. All residual reaction products were stopped in the target layers. γ rays from excited states were measured employing the HORUS γ-ray array [50] comprising 14 HPGe detectors, six of them equipped with BGO Compton suppression shields. The detectors are positioned on the eight corners and six faces of a cube geometry. The count rate of the individual HPGe crystals was maintained around 18 kHz during the experiment.

Compared to preceding α-induced reactions [29–31] a ^{11}B beam is better suited for the population of the high-spin regime. Nevertheless, at a beam energy of 54 MeV, several fusion-evaporation codes compute the relative cross section for the population of ^{131}Xe to be in the range of less than 1%. A detection of evaporated charged particles is imperative to cope with the large background emerging from the dominating ^{131,130}Cs neutron evaporation channels. By setting a gate on evaporated charged particles, the peak to background ratio for the $p3n$ channel ^{131}Xe can be enhanced significantly. For this reason, evaporated charged particles were detected with an annular double-sided silicon strip detector (DSSSD) mounted at backward direction covering an angular range from 118° to 163° with respect to the beam axis. The 310-μm thick silicon disk was produced by RADCON Ltd. (Zelenograd, Russia) and mounted and bonded onto printed circuit boards at the University of Lund, Sweden. The active detector area is divided into 64 radial segments (sectors) on the p-type junction side and into 32 annular segments (rings) on the ohmic n-side facing the target. Each two adjacent ring signals were merged together and read out, in order to distribute the 32 rings to a total of 16 data acquisition channels. Further information and a detailed characterization of the detector are given in Ref. [51]. The DSSSD was shielded against backscattered beam particles by a 25-μm thick tantalum sheet held in place by a 3-μm Tesa® adhesive applied onto a 2-μm polyethylene terephthalate carrier foil [59]. The thickness of the Ta sheet was chosen in such a way that only evaporated protons could reach the Si detector disk.

Coincident events were processed and recorded utilizing the synchronized 80-MHz XIA® Digital Gamma Finder (DGF) data-acquisition system and stored to disk. The data were analyzed offline using the SOCO-V2 [60] and TV [61] codes. A total number of 1.5×10^{10} prompt $\gamma\gamma$ events and 3×10^6 proton-gated $\gamma\gamma$ events were recorded. Events were sorted into (i) a general symmetrized two-dimensional matrix to study $\gamma\gamma$ coincidence relations, (ii) two three-dimensional cubes for DSSSD-Ge-Ge and Ge-Ge-Ge coincidences, and (iii) a total of eight group matrices each corresponding to Ge detector pairs with relative angles $\theta_{1,2} \in \{35, 45, 90, 135, 145\}$ with respect to the beam axis, and angles $\phi \in \{\pm 270, \pm 215, \pm 180, \pm, 55, 0\}$ between the planes spanned by the Ge detectors and the beam axis to investigate multipolarities via angular correlations. Spins of populated states are investigated with the $\gamma\gamma$ angular-correlation code CORLEONE [62, 63] employing the DCO (directional correlation from oriented states) based on the phase convention by Krane, Steffen, and Wheeler [64, 65]. Different hypotheses of involved spins J_1, J_2, J_3 and multipole-mixing ratios δ_1, δ_2 of two coincident γ rays in a cascade $J_1 \xrightarrow{\delta_1} J_2 \xrightarrow{\delta_2} J_3$ are evaluated in χ^2 fits of the correlation function $W(\theta_1, \theta_2, \phi) \equiv W(J_1, J_2, J_3, \delta_1, \delta_2, \sigma)$ on experimental intensities in the different angular-correlation groups. The width of the distribution of the magnetic substates m, i.e. the width of the alignment distribution, was found to be constant at $\sigma = 2.6$. More details on the angular-correlation analysis with CORLEONE are given in Refs. [66, 67].

III. RESULTS

The final level scheme of ^{131}Xe deduced from the three experiments is presented in Fig. 2. It is based on $\gamma\gamma$ coincidences, relative transition intensities, and an angular-correlation analysis. Energies of γ-ray transitions and excitation energies are given in keV. Intensities of γ-ray transitions above the $J^\pi = 11/2^-_1$ isomeric state are extracted from the HORUS experiment and normalized to the 642-keV transition. Newly assigned γ-ray transitions are marked with asterisks.

The beam-like Doppler-corrected singles γ-ray spectra of ^{131}Xe from the ^{136}Xe + ^{208}Pb and ^{136}Xe + ^{238}U AGATA experiments are shown in Figs. 3(a) and 3(c), respectively. The corresponding Xe mass distributions are depicted in the insets Figs. 3(b) and 3(d). Random background is significantly suppressed by gating on the prompt peak in the time-difference distribution between AGATA and PRISMA. Prominent transitions are marked with dotted lines to guide the eye. Energies, spin/parity assignments and relative in-beam intensities of transitions in ^{131}Xe, observed in both AGATA experiments, are summarized in the right part of Tab. I. Efficiency-corrected relative in-beam intensities in Tab. I were determined for the ^{136}Xe + ^{208}Pb experiment and normalized to the 642-keV transition. In total, the γ-ray spectra exhibit eight hitherto known peaks and nine new transitions. None of the known low-spin positive-parity excited states below 2 MeV [30, 31] were populated. γ rays with energies of 188, 389, 642, 810, 901 and 992 keV depopulating the hitherto known positive- and negative-parity states [31] above the $J^\pi = 11/2^-_1$ isomer are clearly visible in the spectra. In addition, the decays of the $J^\pi = 21/2^+_1$ and $17/2^-_1$ states at energies of 444 and 794 keV are observed in the MNT experiments. The peaks at 230, 473, 609, 634, 662, 671, 700, 915, and 1131 keV are candidates for new transitions in ^{131}Xe.

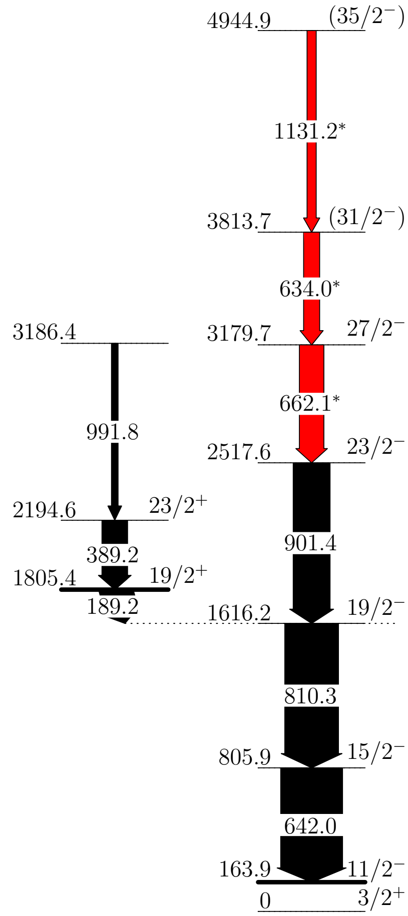

Figure 2. (Color online) Level scheme assigned to ^{131}Xe in the present study. Transition and excitation energies are given in keV. Intensities of the cascades above the 164-keV isomer are deduced from the HORUS experiment and normalized to the 642-keV transition. New γ-ray transitions are marked in red with asterisks. See text for details.

In the ^{11}B + ^{124}Sn fusion-evaporation experiment, a particle trigger is crucial to cope with the significant contribution from xn evaporation channels in order to achieve clean gating conditions for a $\gamma\gamma$ coincidence analysis. The projection of the proton-gated $\gamma\gamma$ matrix is shown in Fig. 3(e). Evaporation residues are identified and selected in the matrix depicted in inset 3(f), where the energy detected by the DSSSD is plotted versus the HORUS γ-ray energy. Evaporated protons are expected in an energy range of approx. 1 to 6 MeV. Low-energy random coincidences are mainly caused by the detection of low-energy δ electrons and β particles. A gate on proton energies larger than 1 MeV is applied; in the resulting $\gamma\gamma$ projection several transitions of the proton-evaporation channels ^{130,131}Xe are well visible above the background. Remaining contaminant transitions from Cs and Pt isotopes are marked by symbols in Fig. 3(e).

The intensities of the coincident γ rays in the HORUS

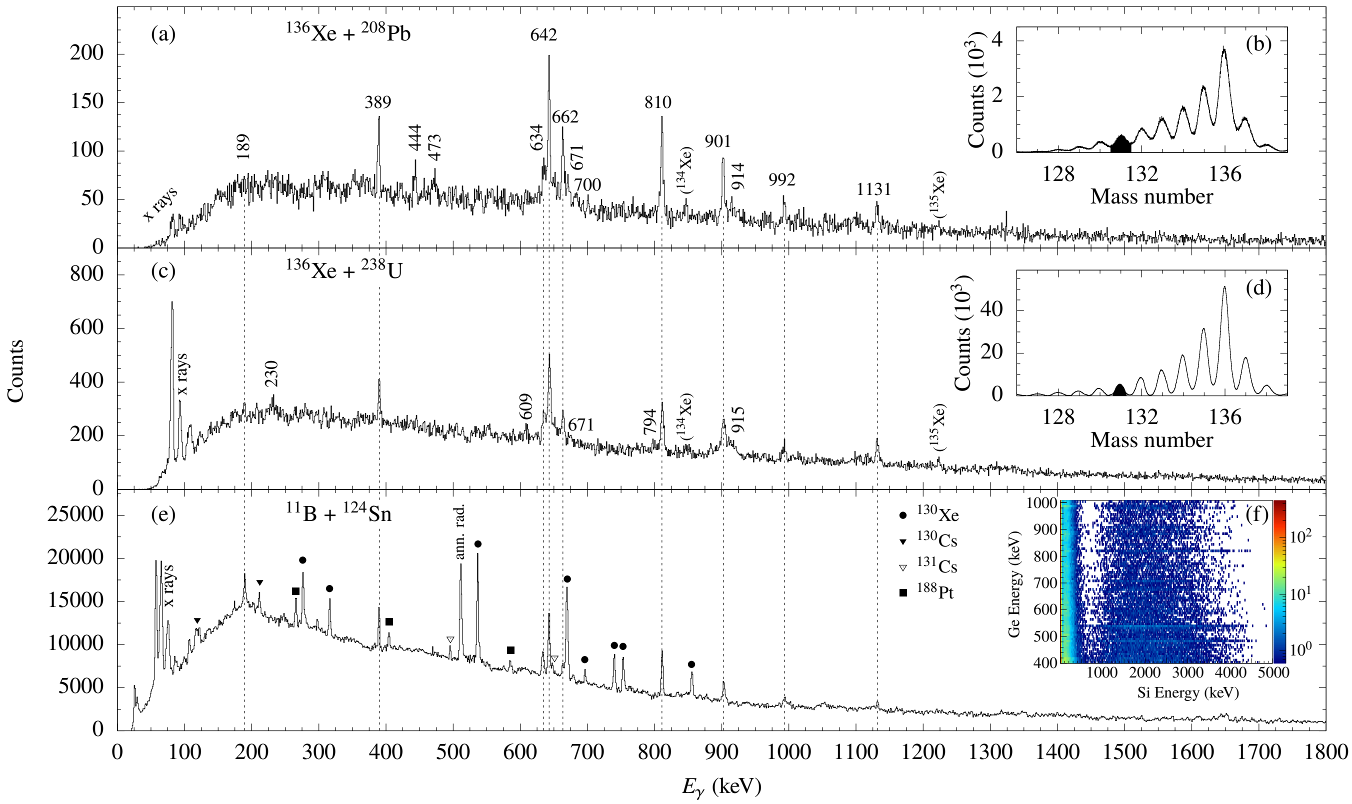

Figure 3. (Color online) (a) Doppler-corrected γ-ray spectrum gated on ^{131}Xe identified with PRISMA in the ^{136}Xe+^{208}Pb experiment. Random background is subtracted with a gate on the prompt peak in the spectrum of time differences between AGATA and PRISMA. (c) Similar data from the ^{136}Xe+^{238}U experiment. Both insets (b) and (d) represent the mass spectra of the Xe isotopes obtained with PRISMA. The applied mass gates for ^{131}Xe are marked black. (e) Projection of the $\gamma\gamma$ matrix gated on evaporated protons (cf. inset (f)) obtained in the HORUS fusion-evaporation reaction ^{11}B + ^{124}Sn. Remaining contaminant transitions are marked with symbols and dominant transitions from ^{131}Xe are marked with dashed lines to guide the eye.

experiment are summarized in the left part of Tab. I. All intensities are efficiency corrected and normalized to the intensity of the 642-keV transition. The uncertainties in the transition energies are ± 0.5 keV. Spin/parity assignments are supported by systematics, shell-model calculations and angular-correlation measurements. Various HORUS prompt $\gamma\gamma$-coincidence spectra are shown in Figs. 4(a) to 4(g). The decay of the $J^\pi = 11/2^-_1$ isomer is not observed due to its long half-life of 11.8 days [28]. Figure 4(a) presents the γ-ray spectrum with a gate on the 642-keV transition. Coincidences are labeled with filled arrow heads. The spectrum exhibits anticipated coincidences at 810, 901, 189, 389 and 992 keV. Beside transitions from ^{130,131}Cs, contaminant peaks are caused by the ground-state band of ^{188}Pt [68] stemming from a dominant fusion-evaporation reaction in the ^{181}Ta backing of the target. All three known γ rays in the positive-parity band with energies of 189, 389 and 992 keV are mutually coincident in the HORUS experiment and were arranged according to their intensity balance as proposed by Kerek *et al.* [31]. Unassigned peaks at 634, 662, and 1131 keV, observed in both AGATA experiments, are coincident to the 642-keV transition. The γ-ray transitions are also in coincidence with the 810-keV transition in Fig. 4(b). Previously, a 901-keV transition was placed parallel to the 3186 keV $\xrightarrow{992\text{ keV}} 23/2^+_1 \xrightarrow{389\text{ keV}} 19/2^+_1 \xrightarrow{189\text{ keV}} 19/2^-_1$ cascade, depopulating the 2518-keV state. A gate on the 901-keV transition is shown in Fig. 4(c). Coincidences as well as the intensity balance require the newly-observed 662-, 634- and 1131-keV transitions to be placed above the 2518-keV state. Gates on those newly observed transitions are shown in Figs. 4(d) to 4(f). All three γ rays are mutually coincident and, thus, form a cascade. The intensity balance in the $\gamma\gamma$ projection gated on the 901-keV transition suggests that the 662-keV transition is directly feeding the 2518-keV state. The intensity of the 634-keV γ-ray peak in the $\gamma\gamma$-coincidence spectrum gated on 901 and 662 keV exceeds the one of the 1131-keV line. In accordance with the intensity balance, the 634-keV transition is placed on top of the newly discovered state at 3180 keV to form the new 3814-keV state. The 1131-keV transition is placed on

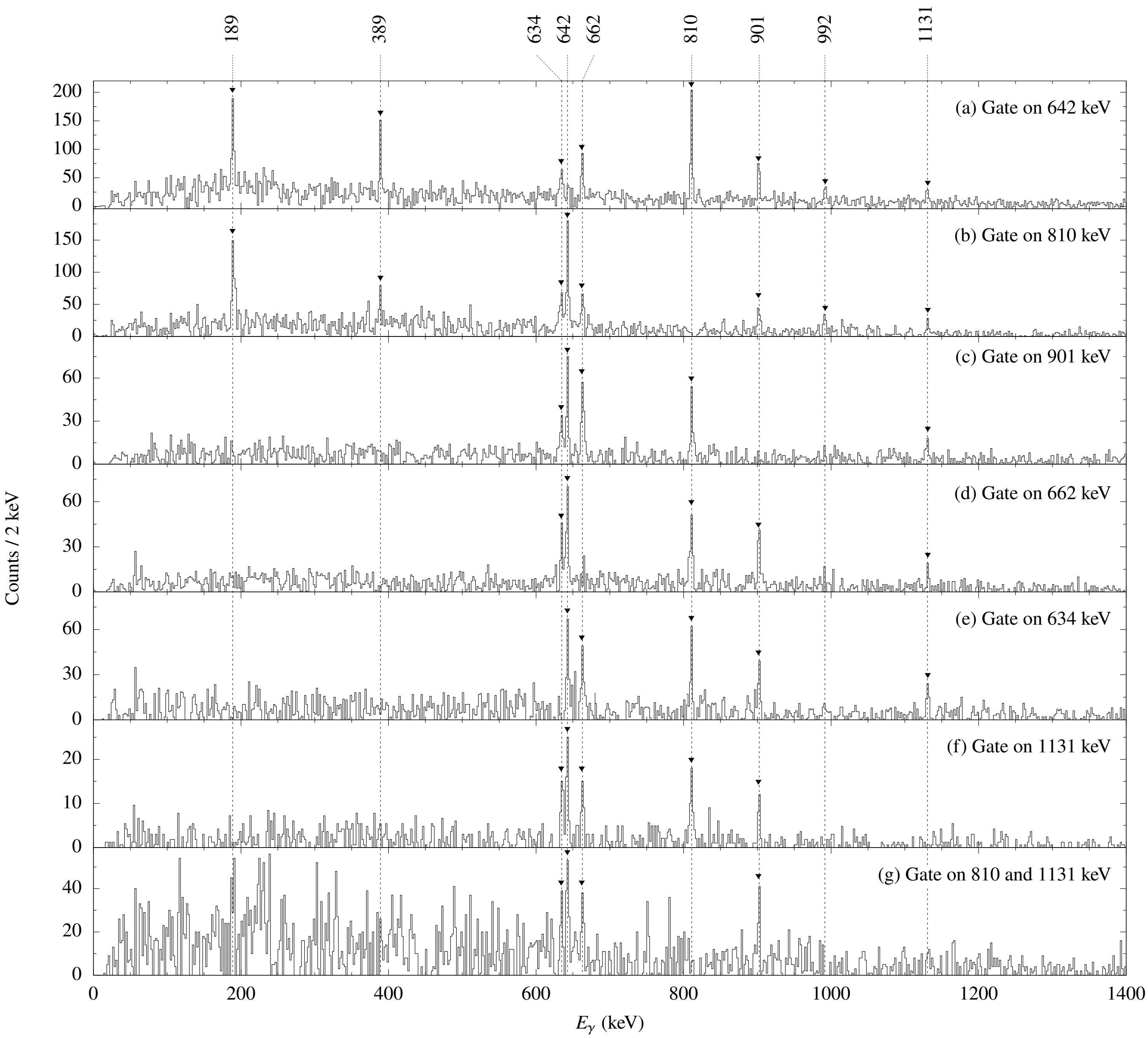

Figure 4. Prompt HORUS $\gamma\gamma$-double and $\gamma\gamma\gamma$-triple coincidence-spectra with gates on (a) 642, (b) 810, (c) 901, (d) 662, (e) 634, (f) 1131, and (g) 810 & 1131 keV. Thin grey lines mark peak energies identified in both MNT experiments (see Tab. I). Coincidences are labeled by filled arrow heads.

top of the cascade to establish a new state at 4945 keV. Furthermore, the intensity balance of the three new γ rays determined in the AGATA experiment confirms this assignment. Also the $\gamma\gamma\gamma$-triple coincidence spectrum with gates on both the 810- and 1131-keV transitions supports a placement of the transitions on top of the 2518-keV state. The maximum excitation energy of approx. 5 MeV is consistent with other populated reaction channels in both AGATA@LNL experiments [39, 69, 70]. Unassigned γ-ray transitions observed with AGATA and listed in Tab. I do not yield meaningful γ-γ coincidences in the HORUS experiment. A placement in the level scheme is not feasible.

In the HORUS experiment spins and parities of excited states are investigated utilizing the angular-correlation analysis described in Sec. II B. A fit of the theoretical angular-distribution function $W(\theta_1, \theta_2, \phi)$ to the experimental intensities of two coincident γ-ray transitions deduced from gates on depopulating transitions in the $\gamma\gamma$ matrices related to the eight angular-correlation groups are performed for each spin hypothesis. To benchmark the validity of the angular correlation analysis, a fit of the $13^+ \rightarrow 12^+$ 417-keV transition in the well populated ^{130}Cs channel is shown in Fig. 5(a). The obtained multipole-mixing ratio $\delta_{\mathrm{exp.}} = -0.11(4)$ reproduces the evaluated value $\delta_{\mathrm{lit.}} = -0.14(6)$ [71]. A further benchmark angular-correlation distribution of the 810-keV transition in ^{131}Xe, gated on the 642-keV transition, is shown in Fig. 5(b). The multipolarity of the 642-keV γ ray is fixed to an $E2$ character, while the spin of the 1616-keV state is tested with values of $J = 15/2$, $17/2$, and $19/2$. Obviously, a pure $E2$ hypothesis yields best results. Figure 5(c) shows the angular-correlation distribution of the 901-810-keV cascade in ^{131}Xe. Spin hypotheses of $J = 19/2$, $21/2$ and $23/2$ were tested for the 2518-keV state. Overall, the $J^{\pi} = 23/2^{-}$ hypothesis matches the experimental values best ($\chi^2 = 1.7$). The previous tentative spin-parity assignment of $J^{\pi} = 21/2^{-}$ [31] has to be revised. Using the same method, the spin of the newly established excited state at 3180 keV is determined. The angular distribution of the 662-keV decay is shown in Fig. 5(d). The $J = 23/2$ and $25/2$ spin hypotheses show discrepancies between the experimental and the calculated intensities in several correlation groups leading to $\chi^2 = 3.1$ and $\chi^2 = 2.9$, respectively. Based on the experimental data, a $J^{\pi} = 27/2^{-}_{1}$ assignment ($\chi^2 = 1.9$) is most appropriate. Summarizing, there is strong evidence for an $E2$ character of the 662- and 634-keV transitions. No accurate analysis of the $\gamma\gamma$ angular correlations for the weakly populated excited states at 3814 keV and 4945 keV were possible due to insufficient statistics. However, tentative spin assignments of $(31/2^{-}_{1})$ and $(35/2^{-}_{1})$ are most probable due to isotopic systematics discussed in Sec. IV A.

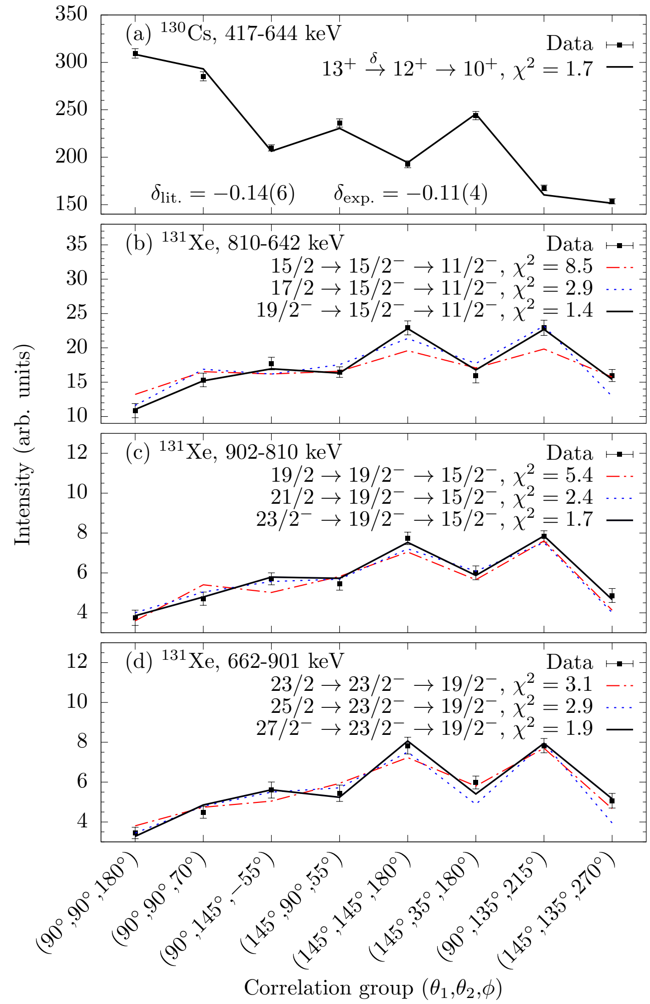

Figure 5. (Color online) $\gamma\gamma$ angular correlations. The experimental intensities (data points) are compared to calculated angular-correlation functions (lines). (a) Fit of the 417-644-keV cascade in ^{130}Cs, (b) of the 810-642-keV, (c) of the 901-810-keV, and (d) of the 662-901 keV cascade in ^{131}Xe. See text for details.

IV. DISCUSSION

A. Systematics along $Z = 54$

Figure 6(a) shows the evolution of the negative-parity yrast band states along the $N = 77$ isotones from Sn to Gd [72–77]. The newly established states of ^{131}Xe are marked with thicker lines. The reevaluated $J^{\pi} = 23/2^{-}_{1}$ state in ^{131}Xe is 7 keV higher in excitation energy compared to the corresponding state in ^{129}Te, thus, the 2518-keV state in ^{131}Xe fits the systematics of $J^{\pi} = 23/2^{-}_{1}$ states from ^{129}Te to ^{133}Ba. In contrast, the previous $J^{\pi} = 21/2^{-}_{1}$ assignment would disrupt the smooth evolution of the $J^{\pi} = 21/2^{-}_{1}$ states in the $N = 77$ isotones. The newly assigned $J^{\pi} = 27/2^{-}_{1}$ state at 3180 keV is located between the excitation energies of the $J^{\pi} = 27/2^{-}_{1}$ states in both neighboring odd-mass nuclei, which further supports the spin assignment. Also the newly assigned states at 3814 and 4945 keV fit into the systematics. Figure 6(b) compares the levels in the favored negative-parity band in ^{131}Xe from the present work with those in the odd-mass nuclei $^{123-129}$Xe [16, 43, 78]. The mid-shell nuclei $^{123-127}$Xe exhibit excitation spectra which are rotational in character. Towards ^{131}Xe a characteristic transition to a vibrational character is observed.

The net. aligned angular momentum $i_x(\omega)$ for the favored negative-parity band along the odd-mass Xe isotopes is presented in Fig. 6(c). The parameter i_x is determined by subtracting the collective part from the total aligned angular momentum: $i_x = I_x - I_{x,\mathrm{coll.}}$ where $I_{x,\mathrm{coll.}} = a\omega + c\omega^3$ follows the parametrization by Harris *et al.* [79]. For ^{133}Xe the collective Harris parametrization fails due to a non-rotational single particle character of this isotope. All Xe isotopes exhibit a pronounced upbend. The crossing frequency at which the alignment occurs is mass-dependent and decreases with increasing mass. A delayed upbend in ^{123,125}Xe takes place at a higher frequency compared to the neighboring nuclei. This behavior is explained by the Pauli blocking of the first pair of $h_{11/2}$ neutrons [42, 43]. In ^{129}Xe a pronounced upbend is found. Huang *et al.* [16] explained the upbend by an alignment of two $h_{11/2}$ protons according to CSM calculations [16]. The negative-parity

Table I. Energies, spin assignments and relative in-beam intensities for transitions observed in ^{131}Xe above the $J^{\pi} = 11/2^{-}_{1}$ isomer at 164 keV. Fitted energies and intensities normalized to the 642-keV transition are taken from the ^{11}B + ^{124}Sn fusion-evaporation experiment and the AGATA ^{136}Xe + ^{208}Pb multinucleon-transfer experiment.

HORUS						AGATA	
E_{γ} (keV)	E_i (keV)	E_f (keV)	I_i^{π}	I_f^{π}	I_{γ}	E_{γ} (keV)	I_{γ}
189.2	1805.4	1616.2	$19/2^{+}$	$19/2^{-}$	29(2)	189	weak
389.2	2194.6	1805.4	$23/2^{+}$	$19/2^{+}$	30(4)	389	41(4)
634.0	3813.7	3179.7	$27/2^{-}$	$23/2^{-}$	24(4)	634	36(3)
642.0	805.9	163.9	$15/2^{-}$	$11/2^{-}$	$\equiv 100$	642	$\equiv 100$
662.1	3179.7	2517.6	$(31/2^{-})$	$27/2^{-}$	32(3)	662	48(4)
810.3	1616.2	805.9	$19/2^{-}$	$15/2^{-}$	87.7(4)	810	78(7)
901.4	2517.6	1616.2	$23/2^{-}$	$19/2^{-}$	58.6(6)	901	60(3)
991.8	3186.4	2194.6	—	$23/2^{+}$	18(3)	992	25(3)
1131.2	4944.9	3813.7	$(35/2^{-})$	$(31/2^{-})$	15(2)	1131	29(2)
—	—	—	—	—	—	230	weak
—	2249.3	1805.4	$21/2^{+}$	$19/2^{+}$	—	444	25(2)
—	—	—	—	—	—	473	19(2)
—	—	—	—	—	—	609	weak
—	—	—	—	—	—	671	15(2)
—	—	—	—	—	—	700	12(2
—	1600	805.9	$17/2^{-}$	$15/2^{-}$	—	794	weak
—	—	—	—	—	—	915	12(2)

band in ^{131}Xe exhibits a large increase of approx. 7 $\hbar$ in aligned angular momentum, accompanied by a decrease of rotational frequency. Similar to the $-2n$ partner, the alignment takes place at the newly established $J^{\pi} = 27/2^{-}_{1}$ state in ^{131}Xe. Since the bandhead of the favored negative-parity band already shows an initial alignment of $J = 11/2\ \hbar$, the observed $h^2_{11/2}$ bandcrossing is blocked, i.e. not the fully aligned 10 $\hbar$ are observed. Following the strong backbending, a remarkable jump back to an alignment of 1 $\hbar$ is observed with the 1131-keV transition.

B. Shell-model calculations

The extended level scheme of ^{131}Xe is confronted with theoretical predictions from five large-scale shell-model calculations in the *gdsh* valence space outside doubly-magic ^{100}Sn.

The first calculation was carried out in the framework of the pair-truncated shell model using a phenomenological interaction, denoted as PQM130 (Pairing+QQ+Multipole for mass region 130). The approach leverages a pairing-plus-quadrupole interaction that consists of spherical single-particle energies, a monopole-pairing, a quadrupole-pairing, and a quadrupole-quadrupole interaction. The Hamiltonian in each neutron and proton space is diagonalized separately and afterwards the total Hamiltonian is diagonalized in the truncated space. More details on the calculation are given in Refs. [17, 80, 81].

The second calculation was carried out employing the computer codes NuShellX@MSU [82] and KSHELL [83] in the untruncated *gdsh* model space with the jj55pna Hamiltonian (referred to as the SN100PN interaction) [84]. The Hamiltonian consists of four parts, treating the neutron-neutron, neutron-proton, proton-proton, and Coulomb repulsion between the protons. The realistic two-body residual interaction is based on a renormalized G matrix derived from the CD-Bonn interaction [85]. The neutron-neutron G-matrix elements, written in the hole-hole formalism, are multiplied by a factor 0.9 to improve results for ^{130}Sn. The proton and neutron single-particle energies are based upon the energy levels in ^{133}Sb and ^{131}Sn.

In addition, a calculation with the effective interaction GCN50:82 [86, 87] was performed with the program KSHELL. Like the SN100PN interaction, the interaction is derived from a realistic G matrix based on the CD-Bonn potential. However, by fitting different combinations of two-body matrix elements to sets of experimental excitation energies from even-even and even-odd semi-magic nuclei, empirical corrections are added to the original G matrix. By using this approach, mainly the monopole part of the interaction is optimized.

Another calculation was conducted in the framework of the Realistic shell model (referred to as Realistic SM) [88]. Single-particle energies and the two-body effec-

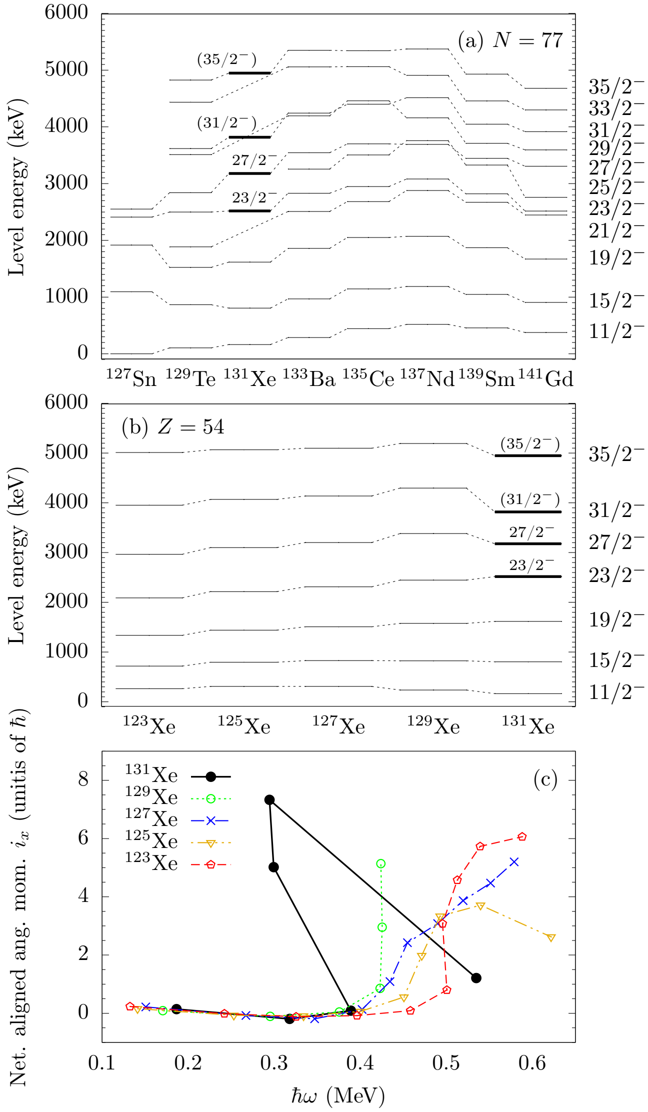

Figure 6. (Color online) Evolution of excited states in the negative-parity band along (a) the odd-mass $N = 77$ isotones from $Z = 50$ to $Z = 64$ [72–77] and along (b) the odd-mass $Z = 54$ isotopes from $N = 69$ to $N = 77$ [16, 43, 78]. Newly discovered states in ^{131}Xe are marked with thick lines. (c) Net. aligned angular momenta $i_x(\hbar)$ of favored negative-parity bands in odd-mass $^{123-131}$Xe isotopes as a function of the rotational frequency $\hbar\omega$.

tive interaction are determined via the $V_{\text{low-}k}$ approach from the CD-Bonn free nucleon-nucleon potential [85] with a cutoff momentum of $\Lambda = 2.6$ fm^{-1}. The effective shell-model Hamiltonian is derived by means of the many-body perturbation theory in the so-called folded-diagram expansion or $\hat{Q}$-box formalism.

The last calculation, called SN100-KTH, is a monopole-optimized realistic interaction, derived via the Monte-Carlo global optimization approach from the G matrix of the CD-Bonn nucleon-nucleon potential [85] by fitting the low-lying states in Sn isotopes. The calculation was performed with the program KSHELL. It was shown that the calculations reproduce well the excitation energies and $E2$ transition probabilities in even-even Te isotopes [89, 90].

Figure 7 compares the experimentally determined energies of the first excited states (Fig. 7(a)) with the results of all five shell-model calculations (Fig. 7(b) PQM130, 7(c) SN100PN, 7(d) GCN50:82, 7(e) Realistic SM, and 7(f) SN100-KTH). The states are separated into columns for the (i) negative- and (ii) the positive-parity states. The angular momentum of the $J^\pi = 3/2^+_1$ ground state is reproduced by the PQM130, GCN50:82, SN100-KTH and Realistic SM interactions, however, the SN100PN interaction reverses the first $J^\pi = 3/2^+_1$ and $1/2^+_1$ states. The $J^\pi = 11/2^-_1$ state with a neutron-hole configuration at 164 keV is best reproduced by the SN100PN, GCN50:82, and SN100-KTH interactions with deviations of only 97, 74 and 27 keV, respectively. The Realistic SM calculation computes the level energy 157 keV too low, while the PQM130 calculation is the only one which predicts the state 137 keV too high. The excitation energies of the first excited positive-parity states $J^\pi = 5/2^+_1$, $7/2^+_1$, $9/2^+_1$, and $11/2^+_1$ are fairly reproduced by all five calculations. The experimental $J^\pi = 13/2^-_1$ state is 239 keV higher in energy with respect to the $J^\pi = 15/2^-_1$ state. SN100PN, SN100-KTH and the Realistic SM calculate the energy differences to be 151, 35, and 115 keV, respectively, while PQM130 and GCN50:82 reverse the ordering of both states. Also the ordering of the first excited $J^\pi = 21/2^+_1$ and $23/2^+_1$ states and of the almost degenerate $J^\pi = 19/2^-_1$ and $17/2^-_1$ states are predicted differently by the five calculations. The experimental energy difference between the $J^\pi = 21/2^+_1$ and $23/2^+_1$ states is 55 keV. This energy difference is predicted slightly larger by the SN100PN, Realistic SM, and the GCN50:82 interactions with deviations of 231, 225 and 292 keV, respectively, while PQM130 transposes both states. The ordering of the $J^\pi = 19/2^-_1$ and $17/2^-_1$ states is predicted correctly by the PQM130, GCN50:82, and SN100-KTH interactions. The calculations suggest that the yet unassigned state on top of the positive-parity band at 3186.4 keV can most likely be interpreted as the first $J^\pi = 25/2^+_1$ or $27/2^+_1$ state. Figure 8 compares the energy differences between experimental and predicted level energies of the five calculations along the favored negative-parity band in greater detail. Going to higher spins ($J^\pi \geq 23/2^-_1$), the energy differences in the different calculations amount up to 747 keV for the $J^\pi = 31/2^-_1$ state. The high-spin states calculated by the SN100PN interaction are more compressed than in the spectra of the other interactions. All five calculations tend to group pairs of spins ($J^\pi = 25/2^-_1$; $27/2^-_1$), ($J^\pi = 29/2^-_1$; $31/2^-_1$) and ($J^\pi = 33/2^-_1$; $35/2^-_1$). Therefore, spin assignments of the newly observed states at 3813.7 ($J^\pi = 31/2^-_1$) and 4944.9 keV ($J^\pi = 35/2^-_1$) are tentative. The SN100PN, GCN50:82, SN100-KTH, and Realistic SM tend to underestimate the excitation energies of states in the high-spin

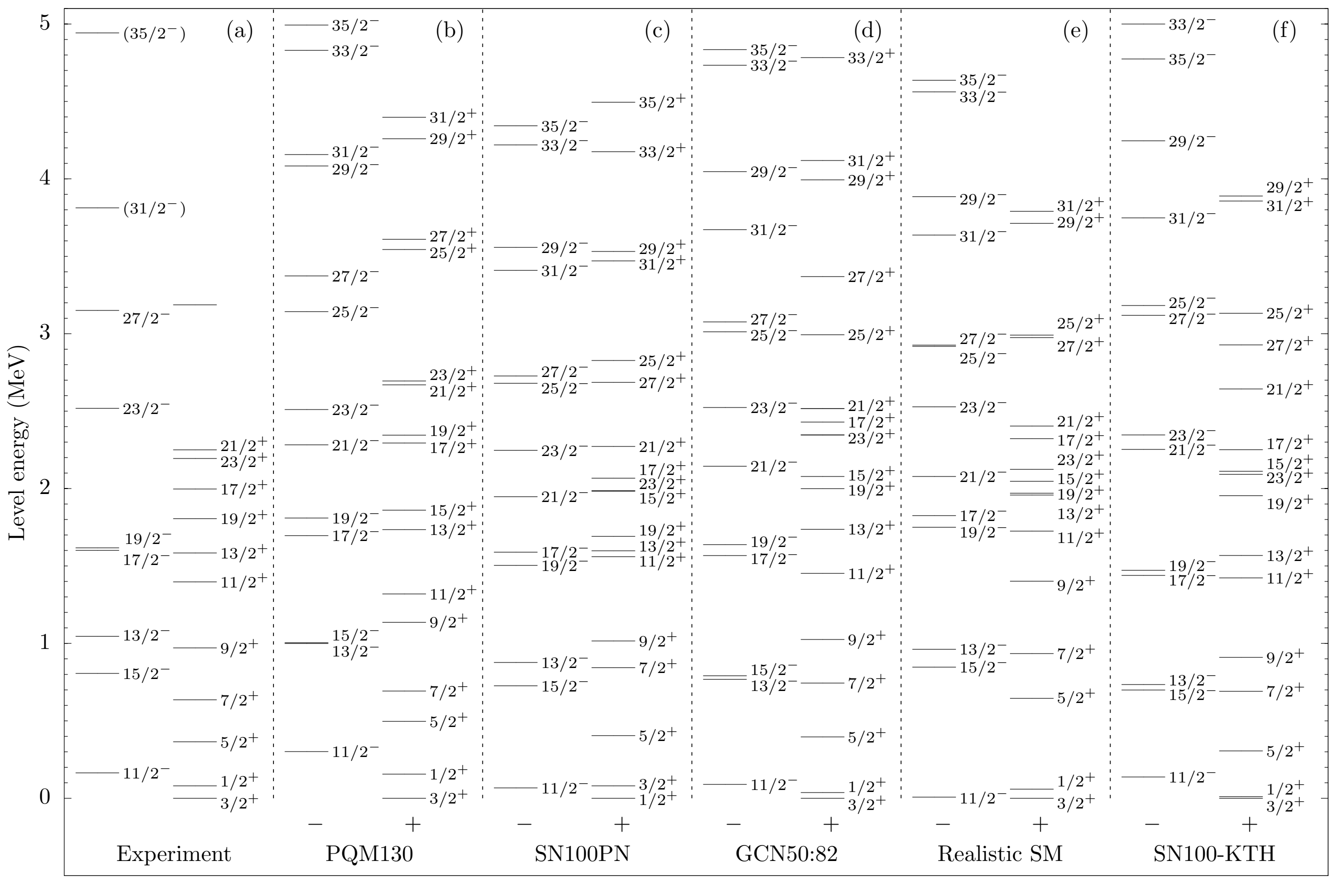

Figure 7. Comparison of experimental energy spectra with the results of shell-model calculations for ^{131}Xe. (a) Experimental energy spectrum. The results obtained with the different interactions are separated in different columns: (b) PQM130, (c) SN100PN, (d) GCN50:82, (e) Realistic SM, and (f) SN100-KTH. For clarity, the states are arranged into two columns for the negative- and the positive-parity states.

regime, while the PQM130 interaction tends to slightly overestimate the excitation energies.

In addition to the excitation energies, reduced transition probabilities were obtained from in the SN100PN and PQM130 calculations. Kerek *et al.* [31] determined the half-life of the $J^\pi = 19/2^+_1$ state in ^{131}Xe at 1805 keV to be 14(3) ns. Neglecting $M2$ contributions, the experimental $B(E1; 19/2^+_1 \to 19/2^-_1)$ value is 4×10^{-6} e^2fm^2, which is consistent with the result of the SN100PN interaction, however, the lower numerical limit for transition strengths in KSHELL is 10^{-4} e^2fm^2. This value fits into the evolution of the half-lives of the $J^\pi = 19/2^+_1$ states along the $N = 77$ isotones. In ^{127}Sn the $J^\pi = 19/2^+_1$ state has a long half-life of 4.52(15) µs [72], while in ^{133}Ba and ^{135}Ce the $J^\pi = 19/2^+_1$ states have half-lives between 2 and 5 ns [91] and 8.2(4) ns [92], respectively. In ^{129}Te no corresponding $J^\pi = 19/2^+_1$ state has been discovered so far.

Furthermore, the isotones along the $N = 77$ chain exhibit several $J^\pi = 23/2^+_1$ isomers. In ^{127}Sn the experimental half-life is 1.19(13) µs [72]. The next odd-mass isotone along the $N = 77$ chain, ^{129}Te, has a $J^\pi = 23/2^+_1$ state with a half-life of 33(3) ns [93]. So far, no experimental indication for a long-lived component of the $J^\pi = 23/2^-_1$ state in ^{131}Xe is reported in the literature. Interestingly, the SN100PN interaction computes the $B(E2; 23/2^+_1 \to 19/2^+_1)$ value to be 6.421 W.u. in ^{131}Xe, corresponding to a lifetime of $\tau \approx 1.4$ ns. Standard effective charges, $e_\pi = 1.5e$ and $e_\nu = 0.5e$, are used in the SN100PN calculation. Furthermore, the PQM130 calculation predicts a $B(E2; 23/2^+_1 \to 19/2^+_1)$ value of 0.348 W.u., corresponding to a lifetime of ≈ 8 ns. Teruya *et al.* uses effective charges of $e_\nu = -1.1$ (due to the neutron-hole character) and $e_\pi = 1.6$.

In order to compare the observed backbending in ^{131}Xe with the odd-mass isotopic neighbors, shell-model calculations were performed for negative-parity states above the $J^\pi = 11/2^-_1$ state in ^{129}Xe. These calculations utilizing the SN100PN interaction are computationally demanding with an m-scheme dimension of 2.4×10^9 for the $J^\pi = 11/2^-_1$ state.

The evolution of the average occupation numbers of the proton and neutron single-particle orbits $\pi h_{11/2}$ and $\nu h_{11/2}$ in the favored negative-parity band of ^{131}Xe, cal-

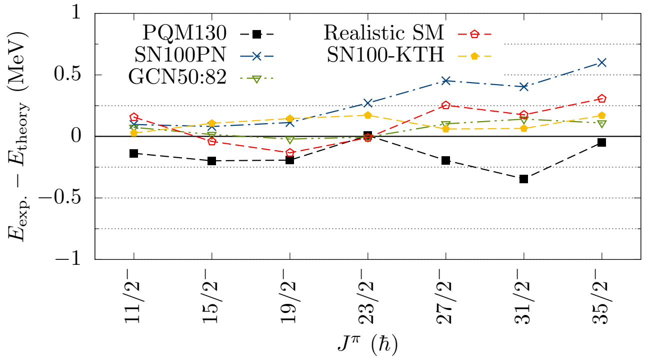

Figure 8. (Color online) Energy differences between experimental and calculated excitation energies with different shell-model interactions plotted against the spin of the state.

culated by the SN100PN and GCN50:82 interactions, are presented in Figs. 9(a)-(d). Similar results from a SN100PN calculation for ^{129}Xe are shown in Figs. 9(e)-(f). Backbending and upbending states in ^{129}Xe and ^{131}Xe are highlighted gray. In ^{131}Xe, both calculations predict a continuous decrease of occupation in the neutron intruder orbital $\nu h_{11/2}$ until it reaches an occupancy of $N_\nu \approx 9$ in the backbending $J^\pi = 27/2^-_1$ state. The decrease of occupation in the $\nu h_{11/2}$ orbital is mainly balanced by the increase of occupation in the $\nu d_{5/2}$ and $\nu g_{7/2}$ orbitals. For higher-lying states ($J^\pi \geq 27/2^-_1$) the $\nu h_{11/2}$ occupation stays constant.

The proton occupancy of the $\pi h_{11/2}$ orbital in ^{131}Xe is predicted to be $N_\pi \approx 0.2$ by both calculations for the $J^\pi = 19/2^-_1$ and $23/2^-_1$ states (Figs. 9(b) and 9(d)). Going to higher spins along the negative-parity band, the proton $\pi h_{11/2}$ occupancy increases. The occupancy is maximal for the backbending states $J^\pi = 27/2^-_1$ and $31/2^-_1$ and decreases again after the alignment. This observation is also in agreement with the results of the Realistic SM calculation were an sharp increase of the $\pi h_{11/2}$ occupancy from 0.14 at the $J^\pi = 23/2^-_1$ state to 0.34 at the $J^\pi = 27/2^-_1$ state is computed. In ^{129}Xe a similar increase of proton occupancy in the $\pi h_{11/2}$ orbital is predicted with the emergence of alignment. The occupation of this configuration persists in the known upbend states with spins $J^\pi \geq 27/2^-_1$. This finding agrees with previous investigations within the framework of the cranked shell model where an alignment of two $h_{11/2}$ protons was proposed recently [16]. Supported by the observation in ^{129}Xe, the proton $h_{11/2}$ configuration in ^{131}Xe has a perturbative but decisive role for the description of the structure of alignment states.

The role of the $\pi h_{11/2}$ orbital is also scrutinized by a detailed decomposition of the states along the favored negative-parity band of ^{131}Xe into their proton and neutron configurations in Figs. 10(a) to 10(f) for the SN100PN interaction and in Figs. 10(i) to 10(n) for the GCN50:82 calculation. All configurations which contribute more than two percent to the overall configuration are shown; the $J^\pi = 15/2^-_1$ state is not visualized for better clarity, nonetheless, the decomposition is very similar to that of the $J^\pi = 11/2^-_1$ state. The percentages of the three most probable configurations are written inside the squares whose areas are proportional to their percentages. The decomposition suggests a highly fragmented structure of ^{131}Xe.

In both calculations, the main components of the $J^\pi = 11/2^-_1$ state (cf. Fig. 10(a) and 10(i)) involve the coupling of the neutron configuration $\nu(h^{-3}_{11/2}d^{-2}_{3/2})$ to the leading proton configurations $\pi(g^4_{7/2})$ and $\pi(g^2_{7/2}d^2_{5/2})$, respectively. The emergence of the two-proton configurations in the $g_{7/2}$ and $d_{5/2}$ orbitals suggests that these two orbitals are energetically close to each other in the proton space. The configuration $\pi(g^2_{7/2}d^2_{5/2})$ is the leading proton configuration for both the $J^\pi = 19/2^-_1$ (24.6% SN100PN; 20.5% GCN50:82) and $J^\pi = 23/2^-_1$ (23.4%; 21.1%) states. In addition, the proton configuration $\pi(g^3_{7/2}d^1_{5/2})$ is gaining significance and is almost equally likely in the $J^\pi = 23/2^-_1$ state (20.0%; 16.9%). In addition to the already mentioned $\nu(h^{-3}_{11/2}d^{-2}_{3/2})$ neutron configurations, a competitive occupation of the $\nu(h^{-3}_{11/2}d^{-1}_{3/2}s^{-1}_{1/2})$ neutron configuration is observed from the $J^\pi = 19/2^-_1$ state onwards.

As discussed and shown in Fig. 6(c), a distinct backbending occurs at rotational frequencies corresponding to the $J^\pi = 27/2^-_1$ and $31/2^-_1$ states. Going from the $J^\pi = 23/2^-_1$ to the $J^\pi = 27/2^-_1$ state, the decomposition matrices of the configurations shown in the panels (d) and (l) of Fig. 10 show once again the emergence of a strong $\pi(g^4_{7/2})$ proton configuration. Simultaneously, the $\pi(g^3_{7/2}d^1_{5/2})$ configuration becomes insignificant. The occupation of two protons in the $g_{7/2}$ and $d_{5/2}$ orbitals (31.9%; 31.5%) is slightly favored over the occupation of four protons in a pure $g_{7/2}$ configuration (22.6%; 11.1%). It is also noteworthy that SN100PN and GCN50:82 predict the proton $h_{11/2}$ orbital to contribute pertubatively to the $J^\pi = 27/2^-_1$ configuration as well, which is consistent with the results presented in Fig. 9(b) and (d).

For the configurations of the $J^\pi = 31/2^-_1$ state shown in Figs. 10(e) and 10(m), a slight rearrangement of the neutron occupancy from the $\nu(h^{-3}_{11/2}d^{-2}_{3/2})$ (23.4%; 31.3%) to the $\nu(h^{-3}_{11/2}d^{-1}_{3/2}s^{-1}_{1/2})$ (19.8%; 23.2%) is predicted by both interactions. Also the contribution of the proton $h_{11/2}$ orbital persists.

Going to higher spins, the configurations become even more fragmented into configurations with less than 2%. As visible in Fig. 6(c), the backbending is completed at the $J^\pi = 35/2^-_1$ state. The change in the nuclear structure is also observed in Figs. 10(f) and 10(n). Configurations with $\pi(g^4_{7/2})$ become negligibly small, while the $\pi(g^3_{7/2}d^1_{5/2})$ configuration, which is negligible small in the backbending region, becomes again a leading configuration. Furthermore, the contribution from the proton

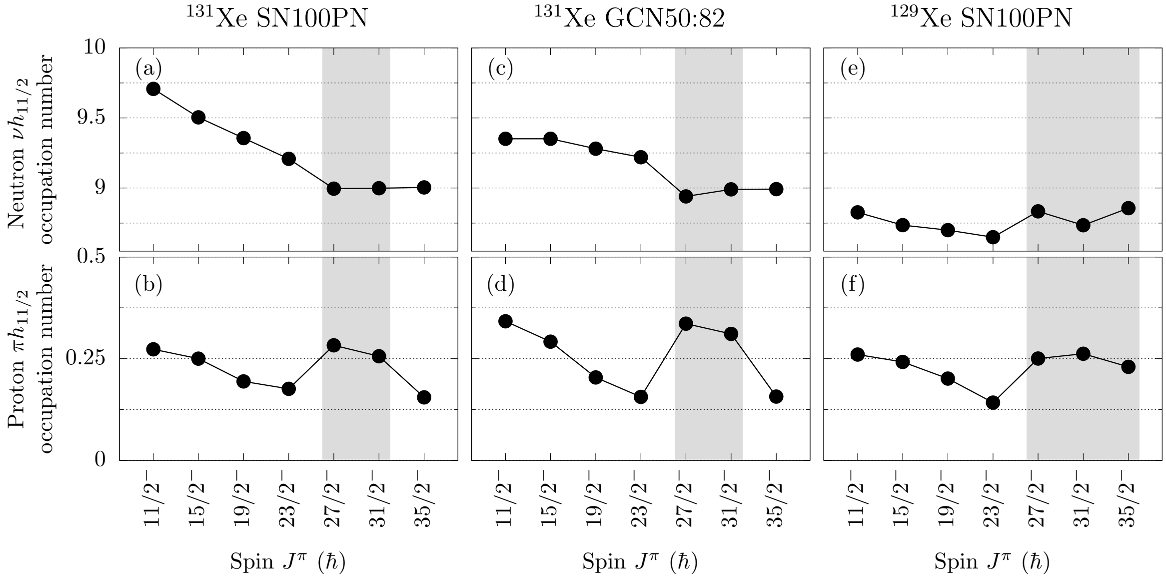

Figure 9. Average neutron (top row) and proton (bottom row) occupation numbers in the proton and neutron $h_{11/2}$ orbitals in ^{131}Xe, calculated with the (a)-(b) SN100PN and (c)-(d) GCN50:82 interaction. (e)-(f) Similar results for ^{129}Xe calculated with the SN100PN interaction.

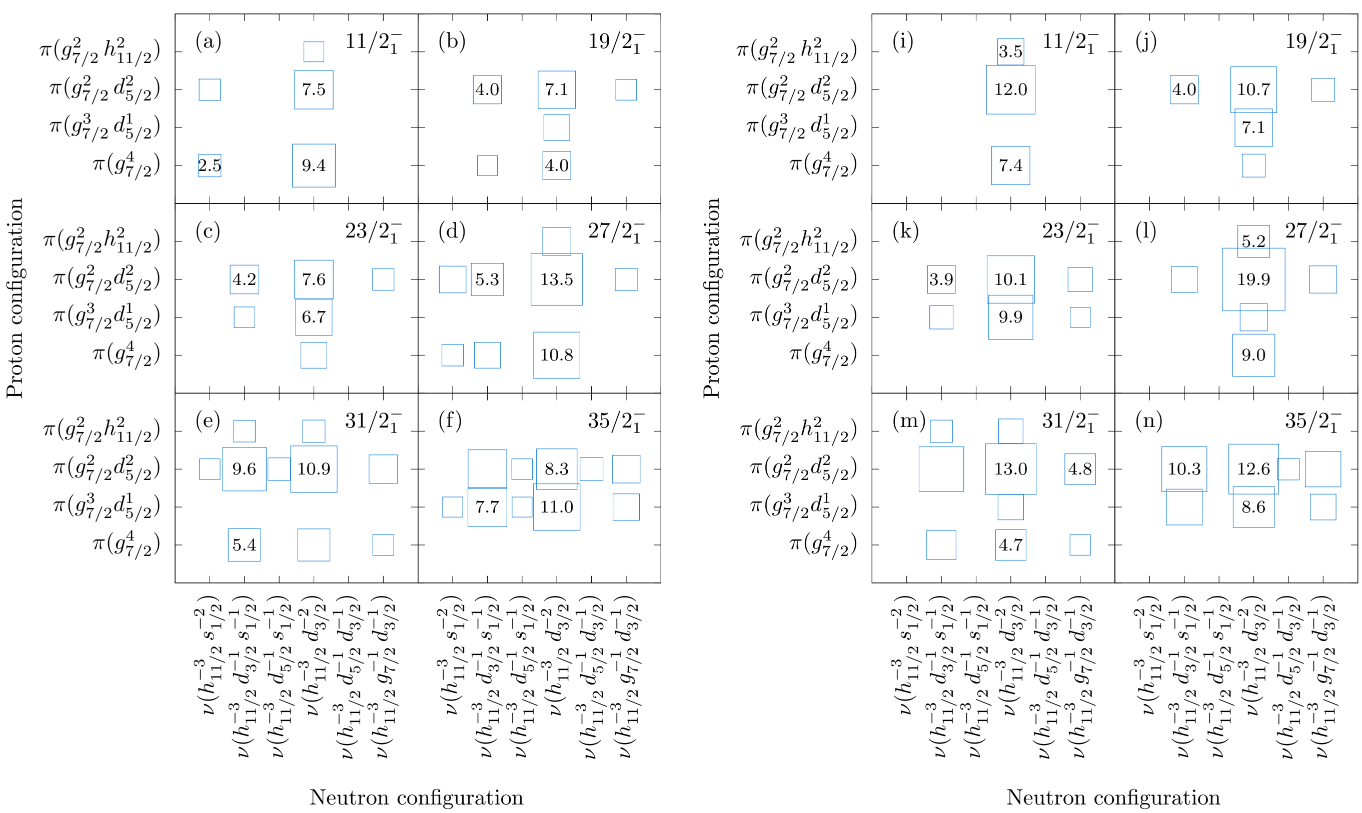

Figure 10. (Color online) Decomposition of selected states of ^{131}Xe into their proton and neutron configurations computed by (a_1)-(f_1) the SN100PN and (a_2)-(f_2) the GCN50:82 interaction. The three largest percentages are written inside the squares. Percentages below 2% are not visualized.

$h_{11/2}$ orbital becomes negligibly small after the alignment at $J^\pi = 35/2^-$.

Figure 11 shows a similar decomposition of the $J^\pi = 23/2^-_1$, $27/2^-_1$, $31/2^-_1$, and $35/2^-_1$ states into their leading proton and neutron configurations, calculated with the SN100PN interaction for ^{129}Xe. Although neutron and proton configurations are more fragmented, the proton configurations before and at the alignment are similar to the ones in ^{131}Xe. Like in ^{131}Xe, the $\pi(g^3_{7/2}d^1_{5/2})$ configuration becomes less probable, while the $\pi h_{11/2}$ configuration contribute pertubatively to the $J^\pi = 27/2^-_1$ and $31/2^-_1$ state in ^{129}Xe. However, deviations occur at the $J^\pi = 35/2^-_1$ state. Unlike in ^{131}Xe (cf. Fig. 10(f,n)), where a strong $\pi(g^3_{7/2}d^1_{5/2})$ character returns to prevail after the backbending, the configurations of the $J^\pi = 35/2^-_1$ state in ^{129}Xe mirror the decompositions observed for the upbend states $J^\pi = 27/2^-_1$ and $31/2^-_1$. In particular the contributions from the $\pi h_{11/2}$ remain unchanged. This behavior confirms the experimentally observed evolution from upbending in ^{129}Xe to the remarkable backbending in ^{131}Xe.

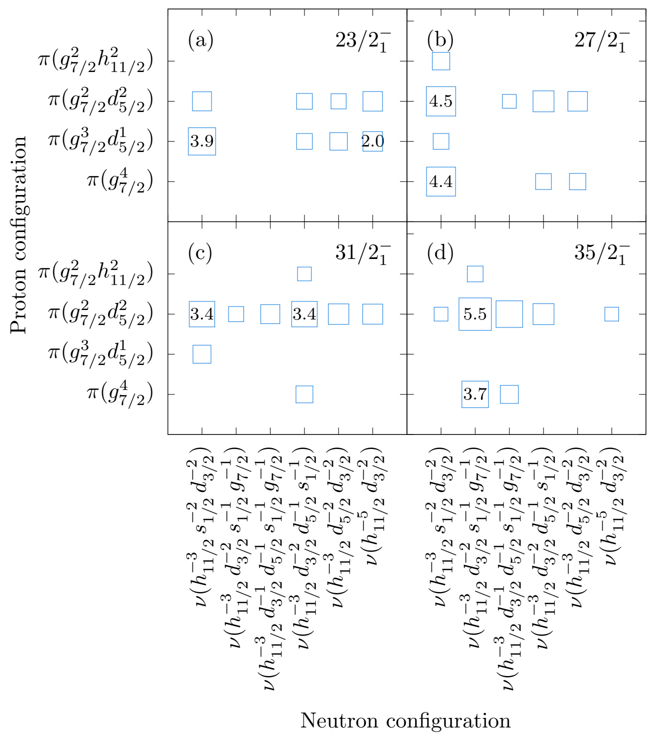

Figure 11. Decomposition of selected states of ^{129}Xe into their proton and neutron configuration computed by the SN100PN interaction.

To inspect the alignment properties and the impact of $\pi h_{11/2}$ protons in ^{131}Xe and ^{129}Xe, the results of the shell-model calculations are reparametrized to the total aligned angular momenta I_x as a function of the rotational frequency $\hbar\omega$. The SN100PN and the GCN50:82 interactions are employed in two separate calculations: (i) permitting excitations into the $\pi h_{11/2}$ orbital and (ii) prohibiting more than one proton in the $\pi h_{11/2}$ orbital. Figure 12(a) compares the extracted theoretical and experimental total aligned angular momenta I_x of ^{131}Xe for calculations without any truncation. The critical frequency at which alignment occurs is slightly underestimated by the Realistic SM and the SN100PN interaction, while the GCN50:82 and SN100-KTH interactions predict the alignment frequency in good agreement with the experiment. The experimentally observed refold to the original Harris fit value with the 1131-keV transition after the alignment is predicted correctly by all calculations, particularly by the GCN50:82 calculation. In fact, all four theoretical calculations provide a fair agreement of the experimental backbending pattern in ^{131}Xe. However, PQM130 does not to reproduce the backbending pattern.

Figure 12(b) compares the extracted theoretical and experimental total aligned angular momenta I_x of ^{131}Xe with the truncation of only one proton in the $\pi h_{11/2}$ orbital. The SN100PN calculation with the $\pi h_{11/2}$ truncation exhibits only a weak upbend, while the truncated GCN50:82 calculation predicts a weakened backbend, both at the position of the $J^\pi = 31/2^-_1$ state. Moreover, both calculations do not reproduce the refolding after the alignment at the $J^\pi = (35/2^-_1)$ state. Consequently, the small increase in the average proton occupancy of the $\pi h_{11/2}$ orbital has significant effects beyond small perturbations.

The same approach is applied to ^{129}Xe. Figure 12(c) compares the experimentally determined I_x curve with untruncated and truncated (only one proton allowed in the $\pi h_{11/2}$ orbital) SN100PN calculations. The critical frequency is again slightly underestimated. A satisfactory reproduction of the experimentally observed upbend is achieved by the untruncated calculation. The truncated calculation does not reproduce the upbend pattern for $J^\pi \leq 31/2^-_1$ states in the yrast band. The LSSM calculation supports the previous explanation of a $\pi h^2_{11/2}$ proton alignment from cranked shell-model calculations in Ref. [16].

Table II. Calculated reduced quadrupole transition strengths $B(E2 : J_i \rightarrow J_{i-2})$ of the favored negative-parity band in ^{131}Xe employing the SN100PN/GCN50:82 interaction with standard effective charges $e_\pi = 1.5e$ and $e_\nu = 0.5e$. The first calculation uses the complete *gdsh* valence space; the second one prohibits more than one proton in the $\pi h_{11/2}$ orbital.

Isotope	Experiment		Theory $B(E2)\downarrow$ $(e^2\text{fm}^4)$	
	E_i(keV)	J^π_i	untruncated	truncated
^{131}Xe	806	$15/2^-_1$	588/530	559/593
	1616	$19/2^-_1$	821/767	601/748
	2518	$23/2^-_1$	932/929	804/883
	3180	$27/2^-_1$	287/30	782/859
	3814	$(31/2^-_1)$	574/306	444/44
	4945	$(35/2^-_1)$	556/346	568/329

The reduced transition strengths $B(E2; J \rightarrow J-2)$ in the vicinity of the backbending region is of special interest. It is well known that in the neighborhood of

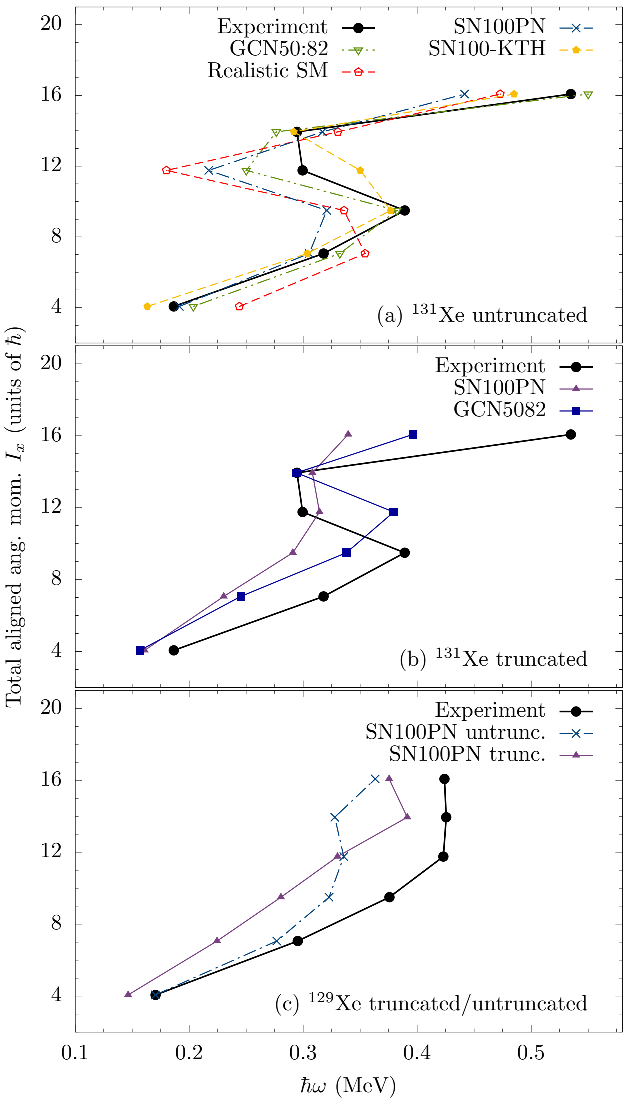

Figure 12. (Color online) (a) Comparison between experimental and calculated total aligned angular momenta I_x as a function of the rotational frequency $\hbar\omega$, employing the SN100PN, GCN50:82, SN100-KTH, and Realistic SM calculations for ^{131}Xe. (b) Comparison between experimental and calculated total aligned angular momenta I_x as a function of the rotational frequency $\hbar\omega$, employing the SN100PN and GCN50:82 with a truncation of only one allowed proton in the $\pi h_{11/2}$ orbital. (c) Similar comparison for ^{129}Xe employing the SN100PN calculation: (i) untruncated and (ii) truncated with only one proton allowed in the $\pi h_{11/2}$ orbital. Experimental data for ^{129}Xe are taken from Ref. [16].

the band crossing a minimum in the $B(E2)$ values is caused by the interaction between the bands [94], therefore, a minimum $B(E2)$ value for the $27/2^-_1 \rightarrow 23/2^-_1$ decay in ^{131}Xe is expected. The $B(E2)$ values calculated for transitions in the yrast band in ^{131}Xe are shown in Tab. II employing the SN100PN and the GCN50:82 interaction with standard effective charges $e_\pi = 1.5e$ and $e_\nu = 0.5e$. The theoretical values are arranged into two columns for the untruncated calculation (left) and the truncated calculation where only one proton is allowed in the $\pi h_{11/2}$ orbital (right). The $B(E2)$ values slightly increase towards the $27/2^-_1 \rightarrow 23/2^-_1$ transition. The SN100PN calculation yields a reduction of the $E2$ transition strength from 932 e^2fm^4 for the decay of the $J^\pi = 23/2^-_1$ state to 287 e^2fm^4 for the decay at the position of the alignment at $J^\pi = 27/2^-_1$. An even more pronounced reduction from 929 e^2fm^4 to 30 e^2fm^4 is calculated by the GCN50:82. A similar result is given by the Realistic SM where the $23/2^-_1 \rightarrow 19/2^-_1$ transition has $B(E2) = 275$ e^2fm^4, compared to $B(E2) = 24$ e^2fm^4 for the $27/2^-_1 \rightarrow 23/2^-_1$ transition. Obviously, this result cannot be reproduced by the truncated calculations without pairs in the $\pi h_{11/2}$ orbital. The alignment and the related reduced $B(E2)$ value is observed for the $J^\pi = 31/2^-_1$ state contradicting the experimental findings. In summary, the reduced transition strengths values provide a precise spin dependent confirmation of the significant role of the $\pi h_{11/2}$ orbital.

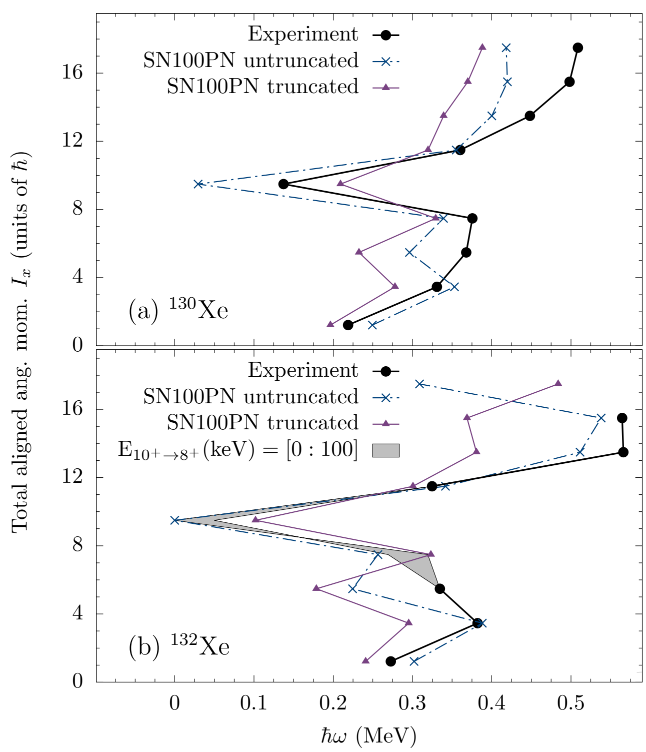

Figure 13. (Color online) (a) Comparison between experimental and calculated total aligned angular momenta I_x as a function of the rotational frequency $\hbar\omega$, employing the SN100PN calculation for (a) ^{130}Xe and (b) ^{132}Xe. The SN100PN interaction is employed in two different calculations: (i) untruncated and (ii) truncated with only one proton allowed in the $\pi h_{11/2}$ orbital. Experimental data taken from Refs. [39, 95].

In order to obtain a consistent picture also the positive-parity ground state bands in the even-even neighbors ^{130}Xe and ^{132}Xe were investigated and calculations employing the SN100PN interaction were carried out. Like before, the calculations are divided into (i) the full *gdsh* valence space and (ii) a truncated calculation where only one proton is allowed to occupy the $\pi h_{11/2}$ orbital. A comparison between the calculations and the experimentally obtained total aligned angular momentum I_x for ^{130}Xe is shown in Fig. 13(a). In ^{130}Xe, I_x smoothly follows the Harris curve up to the $J^\pi = 8_1^+$ state at a rotational frequency of approx. $\hbar\omega = 0.38$ MeV. At the position of the $J^\pi = 10_1^+$ state, I_x exhibits a strong backbending down to a frequency of approx. $\hbar\omega = 0.12$ MeV. Similar to ^{131}Xe, a refolding after the alignment is observed for higher-lying states. Both calculations predict an initial alignment at the position of the $J^\pi = 6_1^+$ state, followed by a strong alignment at the position of the $J^\pi = 10_1^+$ state. The untruncated SN100PN calculation predicts the $J^\pi = 6_1^+$ and 8_1^+ states only 24 keV and 97 keV too low in energy, while the truncated calculation underestimates the energies by 434 keV and 527 keV, respectively. Furthermore, the $J^\pi = 10_1^+$ state at $E_x = 2973$ keV is predicted by the calculations at excitation energies of 2659 keV (untruncated) and 2589 keV (truncated). The occupation of the $\pi h_{11/2}$ orbital decreases from $N_\pi = 0.273$ at the $J^\pi = 0_1^+$ state to $N_\pi = 0.099$ at the $J^\pi = 6_1^+$ state. Subsequently, the occupancy sharply increases to 0.277 at the $J^\pi = 8_1^+$ state and stays almost constant for states with $J^\pi \geq 8_1^+$. The increase of the occupancy is not compatible with the experimentally observed alignment. However, the calculated $B(E2)$ values along the $12_1^+ \rightarrow 10_1^+ \rightarrow 8_1^+ \rightarrow 6_1^+$ cascade drop sharply from 548 e^2fm^4 to 12 e^2fm^4 and rise back to 1084 e^2fm^4. Consequently, all experimental observables are well reproduced corroborating a concurrent neutron and proton alignment in ^{130}Xe. A comparable result was obtained by a theoretical study of the even-mass isotopes $^{114-130}$Xe employing the microscopic sdIBM-2+2q.p. approach [96]. The alignment along the positive-parity band was proposed to be of caused by the $\pi h_{11/2}^2$ proton pair. Rotational alignment of pair of neutrons in the $\nu h_{11/2}^2$ are given by a calculation obtained with the quadrupole-quadrupole-plus-pairing model [34]. These results are in contradiction to the experimental values in ^{130}Xe.

Approaching the $N = 82$ shell closure, a comparison for total aligned angular momenta I_x for ^{132}Xe is depicted in Fig. 13(b). Since no experimental data is available for the $J^\pi = 8^+$ state, the calculation provides a prediction for this state. In order to compare theoretical calculations with the experimental data, I_x is plotted for a range from 0 to 100 keV of the expected transition energy of the yet unobserved $10_1^+ \rightarrow 8_1^+$ decay. The region is marked gray in Fig. 13(b). Both calculations predict a first alignment at the $J^\pi = 6_1^+$ state followed by a second one at the $J^\pi = 10_1^+$ state. Good agreement is obtained with the untruncated calculation where the $J^\pi = 6_1^+$ and 10_1^+ states are slightly underpredicted by 136 and 262 keV, in contrast to the truncated calculation with a discrepancy of 566 keV for the $J^\pi = 6_1^+$ state. The untruncated calculation predicts the $J^\pi = 8_1^+$ state to be degenerated with the $J^\pi = 10_1^+$ state consistent with experimental searches. The truncated calculations predict an energy difference of 204 keV contradicting the experimental observation. In addition, the $(16_1^+) \rightarrow (14_1^+) \rightarrow (12_1^+) \rightarrow (10_1^+)$ cascade with a tentatively assigned 1130-keV transition [39] is in good agreement with the results by the untruncated SN100PN calculation. In ^{132}Xe the alignment is clearly caused by protons in the $\pi h_{11/2}$ orbital.

V. CONCLUSION

In summary, as a main result of three independent measurements and a detailed spectroscopic investigation the level scheme of ^{131}Xe was extended up to an excitation energy of 4945 keV. A pronounced backbending along the negative-parity band on top of the one-quasiparticle $\nu h_{11/2}(\alpha = -1/2)$ band around $\hbar\omega = 0.4$ MeV was observed. The states of the extended negative-parity band closed the gap of unknown high-spin excitations along the isotopic and isotonic chains close to the shell closure at $N = 82$.

Extended large-scale shell-model calculations were performed for ^{131}Xe and its neighbors employing interactions which are applicable in this mass region. In general, the new experimental results, including the pronounced backbending are reproduced by the interactions excluding PQM130. A detailed inspection reveals that only interactions with improved and corrected monopole parts, i.e. GCN50:82 and SN100-KTH, describe the backbending curve and the alignment frequency to its full extent. Comparisons between truncated and untruncated shell-model calculations along the Xe chain in $^{129-132}$Xe clearly indicate that alignment of two $0h_{11/2}$ protons is decisive for the backbending. Calculations of the reduced transition strengths reproduce exactly the spin value where the alignment sets in in ^{131}Xe. The microscopic origin of the alignment in ^{131}Xe was traced back via the wave-function decomposition and its development as a function of angular momentum. The occupation number of the proton $0h_{11/2}$ pair changes significantly at the alignment states in ^{131}Xe providing a distinct signature. Similar results were obtained in the $-2n$ isotope ^{129}Xe. The new results together with previous achievements demonstrate convincingly the predictive power of the modern shell-model calculations with its interaction. The interplay between single-particle and collective excitation in this transitional region arise unambiguously from the specific $h_{11/2}$ intruder orbital.

In future, measurements of lifetimes and g factors which serve as sensitive probes for nucleon alignment, should be performed to reaffirm the proposed backbending mechanism in transitional Xe isotopes. Specifically, the discovery of the predicted nearly degenerated $J^\pi = 8^+$ state in ^{132}Xe, causing the isomeric $J^\pi = 10^+$ state, is of highest interest. Furthermore, fast-timing measurements are in order to resolve the possible onset of $J^{\pi} = 23/2^{+}_{1}$ isomerism in ^{131}Xe which is also predicted by shell-model calculations.

ACKNOWLEDGMENTS

We thank the IKP FN Tandem accelerator team for the professional support during the experiment. We also would like to thank Prof. Dr. Alfredo Poves for providing the GCN50:82 interaction. Furthermore, we express our thanks to Prof. Dr. Furong Xu and Prof. Dr. Costel Petrache for valuable discussions. The research leading to these results has received funding from the German BMBF under contract No. 05P12PKFNE TP4, from the European Union Seventh Framework Programme FP7/2007-2013 under Grant Agreement No. 262010 - ENSAR, from the Spanish Ministerio de Ciencia e Innovación under contract FPA2011-29854-C04, from the Spanish Ministerio de Economía y Competitividad under contract FPA2014-57196-C5, and from the U.K. Science and Technology Facilities Council (STFC). L.K. and A.V. thank the Bonn-Cologne Graduate School of Physics and Astronomy (BCGS) for financial support. One of the authors (A. Gadea) has been supported by the Generalitat Valenciana, Spain, under the grant PROMETEOII/2014/019 and EU under the FEDER program.

[1] R. Wyss, A. Granderath, R. Bengtsson, P. von Brentano, A. Dewald, A. Gelberg, A. Gizon, J. Gizon, S. Harissopulos, A. Johnson, W. Lieberz, W. Nazarewicz, J. Nyberg, and K. Schiffer, "Interplay between proton and neutron S-bands in the Xe-Ba-Ce-region," Nucl. Phys. A **505**, 337 – 351 (1989).

[2] A. Granderath, P.F. Mantica, R. Bengtsson, R. Wyss, P. von Brentano, A. Gelberg, and F. Seiffert, "Shapes and rotational structures of neutron $h_{11/2}$ configurations in the Xe-Ba-Ce region," Nucl. Phys. A **597**, 427 – 471 (1996).

[3] A. Al-Khatib, H. Hübel, P. Bringel, C. Engelhardt, A. Neußer-Neffgen, G. B. Hagemann, C. R. Hansen, B. Herskind, G. Sletten, A. Bracco, F. Camera, G. Benzoni, P. Fallon, R. M. Clark, M. P. Carpenter, R. V. F. Janssens, T. L. Khoo, T. Lauritsen, P. Chowdhury, H. Amro, A. K. Singh, and R. Bengtsson, "Transition to non-collective states at high spin in ^{124}Xe ," Eur. Phys. J **36**, 21–29 (2008).

[4] A. Al-Khatib, A. K. Singh, H. Hübel, P. Bringel, A. Bürger, J. Domscheit, A. Neußer-Neffgen, G. Schönwaßer, G. B. Hagemann, C. Ronn Hansen, B. Herskind, G. Sletten, J. N. Wilson, J. Timár, A. Algora, Zs. Dombrádi, J. Gál, G. Kalinka, J. Molnár, B. M. Nyakó, D. Sohler, L. Zolnai, R. M. Clark, M. Cromaz, P. Fallon, I. Y. Lee, A. O. Macchiavelli, D. Ward, H. Amro, W. C. Ma, M. Kmiecik, A. Maj, J. Styczen, K. Zuber, K. Hauschild, A. Korichi, A. Lopez-Martens, J. Roccaz, S. Siem, F. Hannachi, J. N. Scheurer, P. Bednarczyk, Th. Byrski, D. Curien, O. Dorvaux, G. Duchêne, B. Gall, F. Khalfallah, I. Piqueras, J. Robin, A. Görgen, K. Juhász, S. B. Patel, A. O. Evans, G. Rainovski, G. Benzoni, A. Bracco, F. Camera, S. Leoni, P. Mason, B. Million, A. Paleni, R. Sacchi, O. Wieland, C. M. Petrache, D. Petrache, G. La Rana, R. Moro, G. De Angelis, J. C. Lisle, B. Cederwall, K. Lagergren, R. M. Lieder, E. Podsvirova, W. Gast, H. Jäger, and N. Redon, "Competition between collective and noncollective excitation modes at high spin in ^{124}Ba," Phys. Rev. C **74**, 014305 (2006).

[5] A. K. Singh, H. Hübel, J. Domscheit, G. B. Hagemann, B. Herskind, D. R. Jensen, J. N. Wilson, R. Clark, M. Cromaz, P. Fallon, A. Görgen, I. Y. Lee, A. O. Macchiavelli, D. Ward, H. Amro, W. C. Ma, J. Timár, and I. Ragnarsson, "Evidence for noncollective oblate structures at high spin in ^{123}Cs," Phys. Rev. C **70**, 034315 (2004).

[6] H. Morinaga and N. L. Lark, "Collective excited states in even xenon isotopes," Nucl. Phys. **67**, 315 – 320 (1965).

[7] I. Ragnarsson, A. Sobiczewski, R. K. Sheline, S. E. Larsson, and B. Nerlo-Pomorska, "Comparison of potential-energy surfaces and moments of inertia with experimental spectroscopic trends for non-spherical $Z = 50-82$ nuclei," Nucl. Phys. A **233**, 329 – 356 (1974).

[8] R. Wyss, J. Nyberg, A. Johnson, R. Bengtsson, and W. Nazarewicz, "Highly deformed intruder bands in the $A \approx 130$ mass region," Phys. Lett. B **215**, 211 – 217 (1988).

[9] R. F. Casten and P. von Brentano, "An extensive region of $O(6)$-like nuclei near $A = 130$," Phys. Lett. B **152**, 22 – 28 (1985).

[10] Y. S. Chen, S. Frauendorf, and G. A. Leander, "Shape of rotating quasiparticle orbits and signature splitting in La, Ce, and Pr nuclei," Phys. Rev. C **28**, 2437–2445 (1983).

[11] R. O. Sayer, J. S. Smith, and W. T. Milner, "Rotational and quasirotational bands in even-even nuclei," At. Data Nucl. Data Tables **15**, 85 – 110 (1975).

[12] N. Yoshida, A. Arima, and T. Otsuka, "Description of high-spin states in the interacting boson model," Phys. Lett. B **114**, 86 – 90 (1982).

[13] K. Nomura, T. Nikšić, and D. Vretenar, "Shape-phase transitions in odd-mass γ-soft nuclei with mass $A \approx 130$," Phys. Rev. C **96**, 014304 (2017).

[14] L. M. Robledo, R. R. Rodríguez-Guzmán, and P. Sarriguren, "Evolution of nuclear shapes in medium mass isotopes from a microscopic perspective," Phys. Rev. C **78**, 034314 (2008).

[15] C.-B. Moon, C. S. Lee, T. Komatsubara, Y. Sasaki, and K. Furuno, "Structure of the negative parity bands in ^{125}Xe," Phys. Rev. C **76**, 067301 (2007).

[16] Y. Huang, Z. G. Xiao, S. J. Zhu, C. Qi, Q. Xu, W. J. Cheng, H. J. Li, L. M. Lyu, R. S. Wang, W. H. Yan, H. Yi, Y. Zhang, Q. M. Chen, C. Y. He, S. P. Hu, C. B. Li, H. W. Li, P. W. Luo, X. G. Wu, Y. H. Wu, Y. Zheng, and J. Zhong, "High-spin structures in the ^{129}Xe nucleus," Phys. Rev. C **93**, 064315 (2016).

[17] K. Higashiyama, N. Yoshinaga, and K. Tanabe, "Shell model study of backbending phenomena in Xe isotopes,"

Phys. Rev. C **65**, 054317 (2002).

[18] Y. Lei and Z. Y. Xu, "$(h_{11/2})^2$ alignments in neutron-rich ^{132}Ba with negative-parity pairs," Phys. Rev. C **92**, 014317 (2015).

[19] T. Takahashi, N. Yoshinaga, and K. Higashiyama, "Backbending phenomena in ^{132,134,136}Ce with a pair-truncated shell model," Phys. Rev. C **71**, 014305 (2005).

[20] H. Daniel, O. Mehling, P. Schmidlin, D. Schotte, and E. Thummernicht, "Zerfallsschemata, β-Matrixelemente und γ-Multipolordnungen für die Übergänge ^{56}Co $\rightarrow^{56}$ Fe und ^{131}J $\rightarrow^{131}$ Xe ," Z. Phys **179**, 62–75 (1964).

[21] R. A. Meyer, F. Momyer, and W. B. Walters, "Decay of 8.0-day ^{131}I to levels of ^{131}Xe and 11.77-day ^{131m}Xe ," Z. Phys. **268**, 387–390 (1974).

[22] Chr. Bargholtz, S. Beshai, and L. Gidefeldt, "Angular correlation measurements in ^{131}Xe," Nucl. Phys. A **270**, 189 – 199 (1976).

[23] M.-C. Lépy, L. Brondeau, Ch. Bobin, V. Lourenço, C. Thiam, and M.-M. Bé, "Determination of X- and gamma-ray emission intensities in the decay of ^{131}I," Appl. Radiat. Isot. **109**, 154 – 159 (2016).

[24] M. Berman and G. B. Beard, "Nuclear Resonance Fluorescence in ^{131}Xe," Phys. Rev. C **2**, 1506–1513 (1970).

[25] H. Langhoff, "Lifetime measurements in ^{131}Xe and ^{129}Xe," Nucl. Phys. A **158**, 657 – 663 (1970).

[26] D. C. Hoffman, J. W. Barnes, B. J. Dropesky, F. O. Lawrence, G. M. Kelley, and M. A. Ott, "Half-lives of ^{129m}Xe, ^{131m}Xe, ^{133m}Xe, ^{133g}Xe and ^{135g}Xe," J. Inorg. Nucl. Chem. **37**, 2336 (1975).

[27] D. C. Palmer, A. D. Irving, P. D. Forsyth, I. Hall, D. G. E. Martin, and M. J. Maynard, "Low-lying levels of ^{129}Xe and ^{131}Xe," J. Phys. G **4**, 1143 (1978).

[28] Yu. Khazov, I. Mitropolsky, and A. Rodionov, "Nuclear Data Sheets for $A = 131$," Nucl. Data Sheets **107**, 2715 – 2930 (2006).

[29] A. D. Irving, P. D. Forsyth, I. Hall, and D. G. E. Martin, "The properties of low-lying levels of ^{129}Xe and ^{131}Xe," J. Phys. G **5**, 1595 (1979).

[30] T. Lönnroth, J. Kumpulainen, and C. Tuokko, "One- and Three-Quasiparticle States in ^{127,129,131,133}Xe and Their Coexistence With Band Structures," Phys. Scripta **27**, 228 (1983).

[31] A. Kerek, A. Luukko, M. Grecescu, and J. Sztarkier, "Two- and three-quasiparticle states in ^{132}Xe and ^{131}Xe," Nucl. Phys. A **172**, 603 – 617 (1971).

[32] "Evaluated Nuclear Structure Data File (ENSDF)," (2017), http://www.nndc.bnl.gov/ensdf/.

[33] J. F. Smith, C. J. Chiara, D. B. Fossan, D. R. LaFosse, G. J. Lane, J. M. Sears, K. Starosta, M. Devlin, F. Lerma, D. G. Sarantites, S. J. Freeman, M. J. Leddy, J. L. Durell, A. J. Boston, E. S. Paul, A. T. Semple, I. Y. Lee, A. O. Macchiavelli, and P. H. Heenen, "Excited states and deformation of ^{112}Xe," Phys. Lett. B **523**, 13 – 21 (2001).

[34] S. P. Sarswat, Arun Bharti, and S. K. Khosa, "Backbending and breaking of axial symmetry in the yrast bands of $^{114-130}$Xe isotopes," Phys. Rev. C **58**, 2041–2048 (1998).

[35] H. Kusakari, K. Kitao, K. Sato, M. Sugawara, and H. Katsuragawa, "High-spin states in even-mass Xe nuclei and backbending phenomena," Nucl. Phys. A **401**, 445 – 459 (1983).

[36] C. S. Purry, P.M. Walker, G. D. Dracoulis, T. Kibedi, F. G. Kondev, S. Bayer, A. M. Bruce, A. P. Byrne, W. Gelletly, P. H. Regan, C. Thwaites, O. Burglin, and N. Rowley, "Multi-quasiparticle isomers and rotational bands in ^{178}W," Nuc. Phys. A **632**, 229 – 274 (1998).

[37] H. F. Brinckmann, C. Heiser, and W. D. Fromm, "Ein Hochangeregter isomerer Kernzustand in ^{132}Xe," Nucl. Phys. A **96**, 318 – 326 (1967).

[38] M. v. Hartrott, J. Hadijuana, K. Nishiyama, D. Quitmann, D. Riegel, and H. Schweickert, "Nuclear spin relaxation of Xe in liquid Te," Z. Phys. A **278**, 303–308 (1976).

[39] A. Vogt, M. Siciliano, B. Birkenbach, P. Reiter, K. Hadyńska-Klęk, C. Wheldon, J. J. Valiente-Dobón, E. Teruya, N. Yoshinaga, K. Arnswald, D. Bazzacco, A. Blazhev, A. Bracco, B. Bruyneel, R. S. Chakrawarthy, R. Chapman, D. Cline, L. Corradi, F. C. L. Crespi, M. Cromaz, G. de Angelis, J. Eberth, P. Fallon, E. Farnea, E. Fioretto, C. Fransen, S. J. Freeman, B. Fu, A. Gadea, W. Gelletly, A. Giaz, A. Görgen, A. Gottardo, A. B. Hayes, H. Hess, R. Hetzenegger, R. Hirsch, H. Hua, P. R. John, J. Jolie, A. Jungclaus, V. Karayonchev, L. Kaya, W. Korten, I. Y. Lee, S. Leoni, X. Liang, S. Lunardi, A. O. Macchiavelli, R. Menegazzo, D. Mengoni, C. Michelagnoli, T. Mijatović, G. Montagnoli, D. Montanari, C. Müller-Gatermann, D. Napoli, C. J. Pearson, Zs. Podolyák, G. Pollarolo, A. Pullia, M. Queiser, F. Recchia, P. H. Regan, J.-M. Régis, N. Saed-Samii, E. Şahin, F. Scarlassara, M. Seidlitz, B. Siebeck, G. Sletten, J. F. Smith, P.-A. Söderström, A. M. Stefanini, O. Stezowski, S. Szilner, B. Szpak, R. Teng, C. Ur, D. D. Warner, K. Wolf, C. Y. Wu, and K. O. Zell, "High-spin structures in ^{132}Xe and ^{133}Xe and evidence for isomers along the $N = 79$ isotones," Phys. Rev. C **96**, 024321 (2017).

[40] H. Helppi, J. Hattula, A. Luukko, M. Jääskeläinen, and F. Dönau, "In-beam study of $^{\mathbf{127,129}}$Xe and collective description of the level structures in odd-A Xe nuclei," Nucl. Phys. A **357**, 333 – 355 (1981).

[41] I. Rezanka, A. Kerek, A. Luukko, and C. J. Herrlander, "High-spin states in odd Xe nuclei," Nucl. Phys. A **141**, 130 – 144 (1970).

[42] A. Granderath, D. Lieberz, A. Gelberg, S. Freund, W. Lieberz, R. Wirowski, P. von Brentano, and R. Wyss, "Excited states in ^{125}Xe," Nucl. Phys. A **524**, 153 – 178 (1991).

[43] I. Wiedenhöver, U. Neuneyer, C. Kerskens, J. Altmann, O. Stuch, J. Theuerkauf, G. Siems, R. Wirowski, M. Eschenauer, P. von Brentano, R. Schubart, H. Kluge, and K. H. Maier, "High spin structure in ^{127}Xe and ^{125}Xe," Z. Phys. **347**, 71–72 (1993).

[44] A. Al-Khatib, G. B. Hagemann, G. Sletten, A. K. Singh, H. Amro, G. Benzoni, A. Bracco, P. Bringel, F. Camera, M. P. Carpenter, P. Chowdhury, R. M. Clark, C. Engelhardt, P. Fallon, B. Herskind, H. Hübel, R. V. F. Janssens, T. L. Khoo, T. Lauritsen, A. Neußer-Neffgen, and C. Rønn Hansen, "High-spin spectroscopy in ^{125}Xe," Phys. Rev. C **83**, 024306 (2011).

[45] S. Chakraborty, H. P. Sharma, S. S. Tiwary, C. Majumder, P. K. Prajapati, S. Rai, P. Popli, M. Singh, S. S. Bhattacharjee, R. P. Singh, S. Muralithar, P. Banerjee, S. Ganguly, S. Kumar, A. Kumar, and R. Palit, "Two-Neutron Alignment in ^{127}Xe," Braz. J Phys. **47**, 406–410 (2017).

[46] S. Akkoyun *et al.*, "AGATA – Advanced GAmma Tracking Array," Nucl. Instrum. Meth. Phys. Res. A **668**, 26 (2012).

[47] A. M. Stefanini, L. Corradi, G. Maron, A. Pisent, M. Trotta, A. M. Vinodkumar, S. Beghini, G. Montagnoli, F. Scarlassara, G. F. Segato, A. De Rosa, G. Inglima, D. Pierroutsakou, M. Romoli, M. Sandoli, G. Pollarolo, and A. Latina, "The heavy-ion magnetic spectrometer PRISMA," Nucl. Phys. A **701**, 217 – 221 (2002).

[48] S. Szilner, C. A. Ur, L. Corradi, N. Marginean, G. Pollarolo, A. M. Stefanini, S. Beghini, B. R. Behera, E. Fioretto, A. Gadea, B. Guiot, A. Latina, P. Mason, G. Montagnoli, F. Scarlassara, M. Trotta, G. de Angelis, F. Della Vedova, E. Farnea, F. Haas, S. Lenzi, S. Lunardi, R. Marginean, R. Menegazzo, D. R. Napoli, M. Nespolo, I. V. Pokrovsky, F. Recchia, M. Romoli, M.-D. Salsac, N. Soić, and J. J. Valiente-Dobón, "Multinucleon transfer reactions in closed-shell nuclei," Phys. Rev. C **76**, 024604 (2007).

[49] L. Corradi, S. Szilner, G. Pollarolo, D. Montanari, E. Fioretto, A.M. Stefanini, J. J. Valiente-Dobón, E. Farnea, C. Michelagnoli, G. Montagnoli, F. Scarlassara, C.A. Ur, T. Mijatović, D. Jelavić Malenica, N. Soić, and F. Haas, "Multinucleon transfer reactions: Present status and perspectives," Nucl. Instrum. Meth. Phys. Res. B **317, Part B**, 743 – 751 (2013).

[50] L. Netterdon, V. Derya, J. Endres, C. Fransen, A. Hennig, J. Mayer, C. Müller-Gatermann, A. Sauerwein, P. Scholz, M. Spieker, and A. Zilges, "The γ-ray spectrometer HORUS and its applications for nuclear astrophysics," Nucl. Instrum. Meth. Phys. Res. A **754**, 94 – 100 (2014).

[51] L. Kaya, A. Vogt, P. Reiter, B. Birkenbach, R. Hirsch, K. Arnswald, H. Hess, M. Seidlitz, T. Steinbach, N. Warr, K. Wolf, C. Stahl, N. Pietralla, T. Limböck, K. Meerholz, and R. Lutter, "Characterization and calibration of radiation-damaged double-sided silicon strip detectors," Nucl. Instrum. Meth. Phys. Res. A **855**, 109 – 117 (2017).

[52] A. Gadea, E. Farnea, J. J. Valiente-Dobón, B. Million, D. Mengoni, D. Bazzacco, F. Recchia, A. Dewald, Th. Pissulla, W. Rother, G. de Angelis, *et al.*, "Conceptual design and infrastructure for the installation of the first AGATA sub-array at LNL," Nucl. Instrum. Meth. Phys. Res. A **654**, 88 – 96 (2011).

[53] A. Wiens, H. Hess, B. Birkenbach, B. Bruyneel, J. Eberth, D. Lersch, G. Pascovici, P. Reiter, and H.-G. Thomas, "The AGATA triple cluster detector," Nucl. Instrum. Meth. Phys. Res. A **618**, 223 – 233 (2010).

[54] R.S. Kempley *et al.*, "Cross Coincidences in the ^{136}Xe + ^{208}Pb deep-inelastic reaction," Acta. Phys. Pol. B **42**, 717–720 (2011).

[55] M. Siciliano *et al.*, "Neutron-rich nuclei in the vicinity of ^{208}Pb," LNL Annual Report 2014 **241**, 63–64 (2015).

[56] A. Vogt, B. Birkenbach, P. Reiter, L. Corradi, T. Mijatović, D. Montanari, S. Szilner, D. Bazzacco, M. Bowry, A. Bracco, B. Bruyneel, F. C. L. Crespi, G. de Angelis, P. Désesquelles, J. Eberth, E. Farnea, E. Fioretto, A. Gadea, K. Geibel, A. Gengelbach, A. Giaz, A. Görgen, A. Gottardo, J. Grebosz, H. Hess, P. R. John, J. Jolie, D. S. Judson, A. Jungclaus, W. Korten, S. Leoni, S. Lunardi, R. Menegazzo, D. Mengoni, C. Michelagnoli, G. Montagnoli, D. Napoli, L. Pellegri, G. Pollarolo, A. Pullia, B. Quintana, F. Radeck, F. Recchia, D. Rosso, E. Şahin, M. D. Salsac, F. Scarlassara, P.-A. Söderström, A. M. Stefanini, T. Steinbach, O. Stezowski, B. Szpak, Ch. Theisen, C. Ur, J. J. Valiente-Dobón, V. Vandone, and A. Wiens, "Light and heavy transfer products in ^{136}Xe+^{238}U multinucleon transfer reactions," Phys. Rev. C **92**, 024619 (2015).

[57] B. Bruyneel, B. Birkenbach, and P. Reiter, "Pulse shape analysis and position determination in segmented HPGe detectors: The AGATA detector library," Eur. Phys. J. A **52**, 70 (2016).

[58] A. Lopez-Martens, K. Hauschild, A. Korichi, J. Roccaz, and J-P. Thibaud, "γ-ray tracking algorithms: a comparison," Nucl. Instrum. Meth. Phys. Res. A **533**, 454 – 466 (2004).

[59] tesa SE, "tesa® adhesive 68556 data sheet," .

[60] N. Saed-Samii, *Lifetime measurements using the FATIMA array in combination with EXOGAM@ILL*, Diplomarbeit, Universität zu Köln (2013), unpublished.

[61] J. Theuerkauf, Ph.D. thesis, Universität zu Köln (1994).

[62] I. Wiedenhöver, "Computer code CORLEONE," (1997), unpublished.

[63] I. Wiedenhöver, O. Vogel, H. Klein, A. Dewald, P. von Brentano, J. Gableske, R. Krücken, N. Nicolay, A. Gelberg, P. Petkov, A. Gizon, J. Gizon, D. Bazzacco, C. Rossi Alvarez, G. de Angelis, S. Lunardi, P. Pavan, D. R. Napoli, S. Frauendorf, F. Dönau, R. V. F. Janssens, and M. P. Carpenter, "Detailed angular correlation analysis with 4π spectrometers: Spin determinations and multipolarity mixing measurements in ^{128}Ba," Phys. Rev. C **58**, 721–728 (1998).

[64] K. S. Krane and R. M. Steffen, "Determination of the $E2/M1$ Multipole Mixing Ratios of the Gamma Transitions in ^{110}Cd," Phys. Rev. C **2**, 724–734 (1970).

[65] K.S. Krane, R.M. Steffen, and R.M. Wheeler, "Directional correlations of gamma radiations emitted from nuclear states oriented by nuclear reactions or cryogenic methods," At. Data Nucl. Data Tables **11**, 351 – 406 (1973).

[66] A. Linnemann, *Das HORUS-Würfelspektrometer und Multiphononanregungen in ^{106}Cd*, Ph.D. thesis, Universität zu Köln (2006).

[67] L. Bettermann, C. Fransen, S. Heinze, J. Jolie, A. Linnemann, D. Mücher, W. Rother, T. Ahn, A. Costin, N. Pietralla, and Y. Luo, "Candidates for the one-phonon mixed-symmetry state in ^{130}Xe," Phys. Rev. C **79**, 034315 (2009).

[68] S. Mukhopadhyay, D.C. Biswas, S.K. Tandel, L.S. Danu, B.N. Joshi, G.K. Prajapati, Somnath Nag, T. Trivedi, S. Saha, J. Sethi, R. Palit, and P.K. Joshi, "Coexisting shape- and high-K isomers in the shape transitional nucleus ^{188}Pt," Phys. Lett. B **739**, 462 – 467 (2014).

[69] A. Vogt, B. Birkenbach, P. Reiter, A. Blazhev, M. Siciliano, J. J. Valiente-Dobón, C. Wheldon, D. Bazzacco, M. Bowry, A. Bracco, B. Bruyneel, R. S. Chakrawarthy, R. Chapman, D. Cline, L. Corradi, F. C. L. Crespi, M. Cromaz, G. de Angelis, J. Eberth, P. Fallon, E. Farnea, E. Fioretto, S. J. Freeman, A. Gadea, K. Geibel, W. Gelletly, A. Gengelbach, A. Giaz, A. Görgen, A. Gottardo, A. B. Hayes, H. Hess, H. Hua, P. R. John, J. Jolie, A. Jungclaus, W. Korten, I. Y. Lee, S. Leoni, X. Liang, S. Lunardi, A. O. Macchiavelli, R. Menegazzo, D. Mengoni, C. Michelagnoli, T. Mijatović, G. Montagnoli, D. Montanari, D. Napoli, C. J. Pearson, L. Pellegri, Zs. Podolyák, G. Pollarolo, A. Pullia, F. Radeck, F. Recchia, P. H. Regan, E. Şahin, F. Scarlassara, G. Sletten, J. F. Smith, P.-A. Söderström, A. M. Stefanini, T. Steinbach, O. Stezowski, S. Szilner,

B. Szpak, R. Teng, C. Ur, V. Vandone, D. Ward, D. D. Warner, A. Wiens, and C. Y. Wu, "High-spin structure of ^{134}Xe," Phys. Rev. C **93**, 054325 (2016).

[70] A. Vogt, B. Birkenbach, P. Reiter, A. Blazhev, M. Siciliano, K. Hadyńska-Klęk, J. J. Valiente-Dobón, C. Wheldon, E. Teruya, N. Yoshinaga, K. Arnswald, D. Bazzacco, M. Bowry, A. Bracco, B. Bruyneel, R. S. Chakrawarthy, R. Chapman, D. Cline, L. Corradi, F. C. L Crespi, M. Cromaz, G. de Angelis, J. Eberth, P. Fallon, E. Farnea, E. Fioretto, S. J. Freeman, B. Fu, A. Gadea, K. Geibel, W. Gelletly, A. Gengelbach, A. Giaz, A. Görgen, A. Gottardo, A. B. Hayes, H. Hess, R. Hirsch, H. Hua, P. R. John, J. Jolie, A. Jungclaus, L. Kaya, W. Korten, I. Y. Lee, S. Leoni, L. Lewandowski, X. Liang, S. Lunardi, A. O. Macchiavelli, R. Menegazzo, D. Mengoni, C. Michelagnoli, T. Mijatović, G. Montagnoli, D. Montanari, C. Müller-Gatermann, D. Napoli, C. J. Pearson, L. Pellegri, Zs. Podolyák, G. Pollarolo, A. Pullia, M. Queiser, F. Radeck, F. Recchia, P. H. Regan, D. Rosiak, N. Saed-Samii, E. Şahin, F. Scarlassara, D. Schneiders, M. Seidlitz, B. Siebeck, G. Sletten, J. F. Smith, P.-A. Söderström, A. M. Stefanini, T. Steinbach, O. Stezowski, S. Szilner, B. Szpak, R. Teng, C. Ur, V. Vandone, D. D. Warner, A. Wiens, C. Y. Wu, and K. O. Zell, "Isomers and high-spin structures in the $N = 81$ isotones ^{135}Xe and ^{137}Ba," Phys. Rev. C **95**, 024316 (2017).

[71] T. Koike, K. Starosta, C. J. Chiara, D. B. Fossan, and D. R. LaFosse, "Systematic search of $\pi h_{11/2} \otimes \nu h_{11/2}$ chiral doublet bands and role of triaxiality in odd-odd z=55 isotopes: ^{128,130,132,134}Cs," Phys. Rev. C **67**, 044319 (2003).

[72] R. L. Lozeva, G. S. Simpson, H. Grawe, G. Neyens, L. A. Atanasova, D. L. Balabanski, D. Bazzacco, F. Becker, P. Bednarczyk, G. Benzoni, N. Blasi, A. Blazhev, A. Bracco, C. Brandau, L. Cáceres, F. Camera, S. K. Chamoli, F. C. L. Crespi, J.-M. Daugas, P. Detistov, M. De Rydt, P. Doornenbal, C. Fahlander, E. Farnea, G. Georgiev, J. Gerl, K. A. Gladnishki, M. Górska, J. Grębosz, M. Hass, R. Hoischen, G. Ilie, M. Ionescu-Bujor, A. Iordachescu, J. Jolie, A. Jungclaus, M. Kmiecik, I. Kojouharov, N. Kurz, S. P. Lakshmi, G. Lo Bianco, S. Mallion, A. Maj, D. Montanari, O. Perru, M. Pfützner, S. Pietri, J. A. Pinston, Zs. Podolyák, W. Prokopowicz, D. Rudolph, G. Rusev, T. R. Saitoh, A. Saltarelli, H. Schaffner, R. Schwengner, S. Tashenov, K. Turzó, J. J. Valiente-Dobón, N. Vermeulen, J. Walker, E. Werner-Malento, O. Wieland, and H.-J. Wollersheim, "New sub-μs isomers in ^{125,127,129}Sn and isomer systematics of $^{124\text{-}130}$Sn," Phys. Rev. C **77**, 064313 (2008).

[73] A. Astier, M. G. Porquet, Ts. Venkova, Ch. Theisen, G. Duchêne, F. Azaiez, G. Barreau, D. Curien, I. Deloncle, O. Dorvaux, B. J. P. Gall, M. Houry, R. Lucas, N. Redon, M. Rousseau, and O. Stézowski, "High-spin structures of $^{124-131}$Te: Competition of proton- and neutron-pair breakings," Eur. Phys. J. **50**, 1–24 (2014).

[74] S. Juutinen, P. Šimeček, P. Ahonen, M. Carpenter, C. Fahlander, J. Gascon, R. Julin, A. Lampinen, T. Lönnroth, J. Nyberg, A. Pakkanen, M. Piiparinen, K. Schiffer, G. Sletten, S. Törmänen, and A. Virtanen, "Shape coexistence in the transitional ^{133}Ba nucleus," Phys. Rev. C **51**, 1699–1707 (1995).

[75] R. Ma, E. S. Paul, D. B. Fossan, Y. Liang, N. Xu, R. Wadsworth, I. Jenkins, and P. J. Nolan, "Rotational bands in ^{135}Ce: Collective prolate and oblate rotation," Phys. Rev. C **41**, 2624–2634 (1990).

[76] C. M. Petrache, R. Venturelli, D. Vretenar, D. Bazzacco, G. Bonsignori, S. Brant, S. Lunardi, M. A. Rizzutto, C. Rossi Alvarez, G. de Angelis, M. De Poli, and D. R. Napoli, "High-spin states in ^{137}Nd: A large variety of collective rotations," Nucl. Phys. A **617**, 228 – 248 (1997).

[77] S. M. Mullins, A. Omar, L. Persson, D. Prévost, J. C. Waddington, H. R. Andrews, G. C. Ball, A. Galindo-Uribarri, V. P. Janzen, D. C. Radford, D. Ward, T. E. Drake, D. B. Fossan, D. LaFosse, P. Vaska, M. Waring, and R. Wadsworth, "Perturbed alignments within an $i_{13/2}$ neutron intruder band in ^{141}Gd," Phys. Rev. C **47**, R2447–R2451 (1993).

[78] A. Schmidt, I. Schneider, H. Meise, I. Wiedenhöver, O. Stuch, K. Jessen, D. Weisshaar, C. Schumacher, P. von Brentano, G. Sletten, B. Herskind, M. Bergström, and J. Wrzesinski, "High Spin Structure in ^{123}Xe," Eur. Phys. J **2**, 21–23 (1998).

[79] Samuel M. Harris, "Higher Order Corrections to the Cranking Model," Phys. Rev. **138**, B509–B513 (1965).

[80] E. Teruya, N. Yoshinaga, K. Higashiyama, and A. Odahara, "Shell-model calculations of nuclei around mass 130," Phys. Rev. C **92**, 034320 (2015).

[81] Koji Higashiyama and Naotaka Yoshinaga, "Pair-truncated shell-model analysis of nuclei around mass 130," Phys. Rev. C **83**, 034321 (2011).

[82] B. A. Brown and W. D. M. Rae, "The Shell-Model Code NuShellX@MSU," Nucl. Data Sheets **120**, 115 – 118 (2014).

[83] N. Shimizu, "Nuclear shell-model code for massive parallel computation, "KSHELL"," (2013), arXiv:1310.5431 [nucl-ph].

[84] B. A. Brown, N. J. Stone, J. R. Stone, I. S. Towner, and M. Hjorth-Jensen, "Magnetic moments of the 2_1^+ states around ^{132}Sn," Phys. Rev. C **71**, 044317 (2005).

[85] R. Machleidt, "High-precision, charge-dependent bonn nucleon-nucleon potential," Phys. Rev. C **63**, 024001 (2001).

[86] E. Caurier, F. Nowacki, A. Poves, and K. Sieja, "Collectivity in the light xenon isotopes: A shell model study," Phys. Rev. C **82**, 064304 (2010).

[87] E. Caurier, F. Nowacki, and A. Poves, "Shell model description of the $\beta\beta$ decay of ^{136}Xe," Phys. Lett. B **711**, 62 – 64 (2012).

[88] L. Coraggio, L. De Angelis, T. Fukui, A. Gargano, and N. Itaco, "Calculation of gamow-teller and two-neutrino double-β decay properties for ^{130}Te and ^{136}Xe with a realistic nucleon-nucleon potential," Phys. Rev. C **95**, 064324 (2017).

[89] Chong Qi, "Shell-model configuration-interaction description of quadrupole collectivity in te isotopes," Phys. Rev. C **94**, 034310 (2016).

[90] Chong Qi and Z. X. Xu, "Monopole-optimized effective interaction for tin isotopes," Phys. Rev. C **86**, 044323 (2012).

[91] J. Gizon, A. Gizon, and D. J. Horen, "Band structure in ^{131,132,133}Ba observed by (^{12}C,xn) reactions," Nucl. Phys. A **252**, 509 – 523 (1975).

[92] A. Zemel, C. Broude, E. Dafni, A. Gelberg, M. B. Goldberg, J. Gerber, G. J. Kumbartzki, and K. H. Speidel, "Magnetic moment of the $19/2^+$ isomer in ^{135}ce," Z. Phys. A – Atoms and Nuclei **304**, 269–272 (1982).

[93] C. T. Zhang, M. Sferrazza, R. H. Mayer, Z. W. Grabowski, P. Bhattacharyya, P. J. Daly, R. Broda, B. Fornal, W. Królas, T. Pawłat, G. de Angelis, D. Bazzacco, S. Lunardi, and C. Rossi-Alvarez, "Yrast excitations in ^{129}Te," Z. Phys. A **353**, 11–12 (1995).

[94] A. Dewald, "Transition probabilities in transitional nuclei in the A=130 region," Prog. Part. Nucl. Phys. **28**, 409 – 418 (1992).

[95] T. Lönnroth, J. Hattula, H. Helppi, S. Juutinen, K. Honkanen, and A. Kerek, "Study of band crossings in ^{130}Xe," Nucl. Phys. A **431**, 256 – 268 (1984).

[96] Shi Zhu-yi, Liu Yong, and Sang Jian-ping, "The nuclear structure and backbending phenomenon for $^{114-130}$Xe isotopes," Chinese Phys. **10**, 282 (2001).